8-15-2017

Microstructural Alterations and Oligodendrocyte Dysmaturation in White Matter After Cardiopulmonary Bypass in a Juvenile Porcine Model.

Gary R Stinnett

Stephen Lin

Alexandru V Korotcov

Ludmila Korotcova

Paul D Morton

See next page for additional authors

Authors
Gary R Stinnett, Stephen Lin, Alexandru V Korotcov, Ludmila Korotcova, Paul D Morton, Shruti D Ramachandra, Angeline Pham, Sonali Kumar, Kota Agematsu, David Zurakowski, Paul C Wang, Richard A Jonas, and Nobuyuki Ishibashi

ORIGINAL RESEARCH

Microstructural Alterations and Oligodendrocyte Dysmaturation in White Matter After Cardiopulmonary Bypass in a Juvenile Porcine Model

Gary R. Stinnett, PhD; Stephen Lin, MEngr; Alexandru V. Korotcov, PhD; Ludmila Korotcova, MD; Paul D. Morton, PhD; Shruti D. Ramachandra, BS; Angeline Pham, BS; Sonali Kumar, BS; Kota Agematsu, MD; David Zurakowski, PhD; Paul C. Wang, PhD; Richard A. Jonas, MD; Nobuyuki Ishibashi, MD

***Background*—**Newly developed white matter (WM) injury is common after cardiopulmonary bypass (CPB) in severe/complex congenital heart disease. Fractional anisotropy (FA) allows measurement of macroscopic organization of WM pathology but has rarely been applied after CPB. The aims of our animal study were to define CPB-induced FA alterations and to determine correlations between these changes and cellular events after congenital heart disease surgery.

***Methods and Results*—**Normal porcine WM development was first assessed between 3 and 7 weeks of age: 3-week-old piglets were randomly assigned to 1 of 3 CPB-induced insults. FA was analyzed in 31 WM structures. WM oligodendrocytes, astrocytes, and microglia were assessed immunohistologically. Normal porcine WM development resembles human WM development in early infancy. We found region-specific WM vulnerability to insults associated with CPB. FA changes after CPB were also insult dependent. Within various WM areas, WM within the frontal cortex was susceptible, suggesting that FA in the frontal cortex should be a biomarker for WM injury after CPB. FA increases occur parallel to cellular processes of WM maturation during normal development; however, they are altered following surgery. CPB-induced oligodendrocyte dysmaturation, astrogliosis, and microglial expansion affect these changes. FA enabled capturing CPB-induced cellular events 4 weeks postoperatively. Regions most resilient to CPB-induced FA reduction were those that maintained mature oligodendrocytes.

***Conclusions*—**Reducing alterations of oligodendrocyte development in the frontal cortex can be both a metric and a goal to improve neurodevelopmental impairment in the congenital heart disease population. Studies using this model can provide important data needed to better interpret human imaging studies. **(*J Am Heart Assoc*. 2017;6:e005997. DOI: 10.1161/JAHA.117.005997.)**

Key Words: cardiopulmonary bypass • congenital heart disease • diffusion tensor imaging • thoracic surgery • white matter

Hospital mortality for neonates and infants with severe/complex congenital heart disease (CHD) has dramatically improved over the past 2 decades.[1] However, many survivors of complex CHD repair are at significant risk for important neurodevelopmental morbidity.[1-4] Within a wide range of brain regions, newly developed postoperative white matter (WM) injury is common.[5-7] It has been well established that alterations of the WM microstructure persist into later life,[8] and impairments of neural connectivity due to WM injury cause neurological dysfunction including attention deficit, executive dysfunction, impairment of working memory, and verbal dysfunction.[8-10] Because these deficits are remarkably similar to neurodevelopmental morbidity in patients with severe/complex CHD,[3,11,12] it is likely that the extent of abnormal WM development early in life accounts for the type and degree of neurological deficits observed in the CHD population.[13]

From the Children's National Heart Institute (G.R.S., L.K., P.D.M., S.D.R., K.A., R.A.J., N.I.) and Center for Neuroscience Research, Children's National Health System, Washington, DC (G.R.S., L.K., P.D.M., S.D.R., K.A., R.A.J., N.I.); Department of Radiology, Howard University, Washington, DC (S.L., A.V.K., P.C.W.); Center for Neuroscience and Regenerative Medicine, Uniformed Services University, Bethesda, MD (A.V.K.); George Washington University School of Medicine and Health Science, Washington, DC (A.P., S.K., R.A.J., N.I.); Departments of Anesthesia and Surgery, Boston Children's Hospital, Harvard Medical School, Boston, MA (D.Z.); College of Science and Engineering, Fu Jen Catholic University, Taipei, Taiwan (P.C.W.).

Correspondence to: Nobuyuki Ishibashi, MD, or Richard A. Jonas, MD, Children's National Health System, 111 Michigan Avenue, NW, Washington, DC. E-mails: nishibas@childrensnational.org, rjonas@childrensnational.org

Received March 1, 2017; accepted June 15, 2017.

Clinical Perspective

What Is New?

- Our study, using a porcine developmental model, demonstrates the dynamic relationship between fractional anisotropy, the clinically relevant biomarker for studying white matter development and pathology, and cellular events after pediatric cardiac surgery.
- Our analysis identifies region-specific white matter vulnerability to insults associated with cardiac surgery and reveals that white matter regions in the frontal cortex are particularly susceptible after cardiopulmonary bypass.
- In conjunction with detailed cellular assays, the present study suggests that alterations of fractional anisotropy are affected by oligodendrocyte dysmaturation, astrogliosis, and microglial expansion due to cardiopulmonary bypass.

What Are the Clinical Implications?

- Fractional anisotropy in the frontal cortex should be a clinically relevant biomarker in white matter injury after cardiac surgery.
- Reducing and recovering alterations of oligodendrocyte development in the frontal cortex can be both a metric and a goal to improve life-long neurodevelopmental consequences in children with congenital heart disease.

Limited sensitivity and specificity in conventional magnetic resonance imaging (MRI) have prevented direct linking of quantitative/semiquantitative image results with neurological outcomes in CHD.[13] Diffusion tensor imaging (DTI) is a powerful MRI technique that can measure macroscopic organization for studying WM pathology.[14] Fractional anisotropy (FA) obtained from DTI has been widely used to detect a variety of WM injuries and to quantify the pathological state.[15] Indeed, despite scant WM injury evident on conventional MRI, adolescents with d-transposition of the great arteries repaired in infancy had WM regions with significantly lower FA.[16] In those adolescents WM FA reductions were associated with their neurocognitive deficits.[17] The development of innovative image-processing technology is now enabling us to introduce such advanced neuroimaging in the fetus and neonate.[18] Therefore, future clinical imaging studies paired with neurological outcome investigations will greatly assist our understanding of WM damage at a microstructural level and will facilitate correlation with specific developmental and behavioral disabilities in patients with CHD.

There is a clear need for animal studies incorporating clinically relevant imaging approaches paired with histological analysis to CHD-induced brain insults. In conjunction with clinical research, studies of this nature will aid in acquiring a full picture of CHD-induced abnormal WM development and injury and will likely lead to development of novel treatment and management strategies for reduction of neurodevelopmental morbidity in children with severe/complex CHD.

Previous attempts to study WM injury using rodent models have been limited by structural differences with the human brain. In the human brain WM occupies ≈50% of the total brain volume, whereas in rodents it is only 15%.[19] In contrast the piglet brain is a powerful model to study human brain development as it displays a highly evolved, gyrencephalic neocortex structurally similar to the human brain.[20] Furthermore ≈50% of the piglet brain volume is represented by WM.[21] Finally the piglet is large enough in the newborn period for investigation using cardiopulmonary bypass (CPB),[22,23] which can result in unique and specific pathological conditions in the developing brain with CHD.[13] In order to enable improved interpretation of human DTI studies at the cellular level, the aims of the present study were (1) to characterize development of the gyrencephalic WM in a unique developing porcine model; (2) to define alterations of WM microstructures after cardiac surgery with DTI; and (3) to determine correlation of FA changes with CPB-induced cellular events using our histological approach.

Methods

Experimental Model

CPB results in systemic inflammatory response syndrome (SIRS) due to blood exposure to nonendothelial surfaces, such as the artificial oxygenator, tubing, and cannulas.[24] In addition, CHD patients are at greater risk of global cerebral ischemia during CPB, resulting from blood steal syndrome due to aortopulmonary collateral vessels and possible cerebral vessel abnormality.[25,26] Embolism of both solid particles and gaseous emboli due to CPB is also an important cause of ischemia-reperfusion/reoxygenation (I/R) injury.[26] Finally, the circulatory arrest technique still involves risk of I/R-injury such as the "no-reflow phenomenon."[27] To investigate the effects of CPB on WM development, therefore, piglets at 3 weeks of age were randomly assigned to 1 of 3 groups exposed to different CPB-induced brain insults involving I/R injury and SIRS (Figure 1A): (1) control (sham surgery, no CPB-induced insult, n=3); (2) 34°C full-flow bypass for 60 minutes (mild CPB insult, CPB-induced SIRS, n=4); and (3) 25°C circulatory arrest for 60 minutes (severe CPB insult, CPB-induced SIRS with I/R injury, n=6). We performed all experiments in compliance with the NIH *Guide for the Care and Use of Laboratory Animals*. The study was approved by the Animal Care and Use Committee at Children's National Medical Center.

Preparation for Surgery

All animals were sedated with intramuscular ketamine and xylazine and intubated with a 4.5-mm cuffed endotracheal

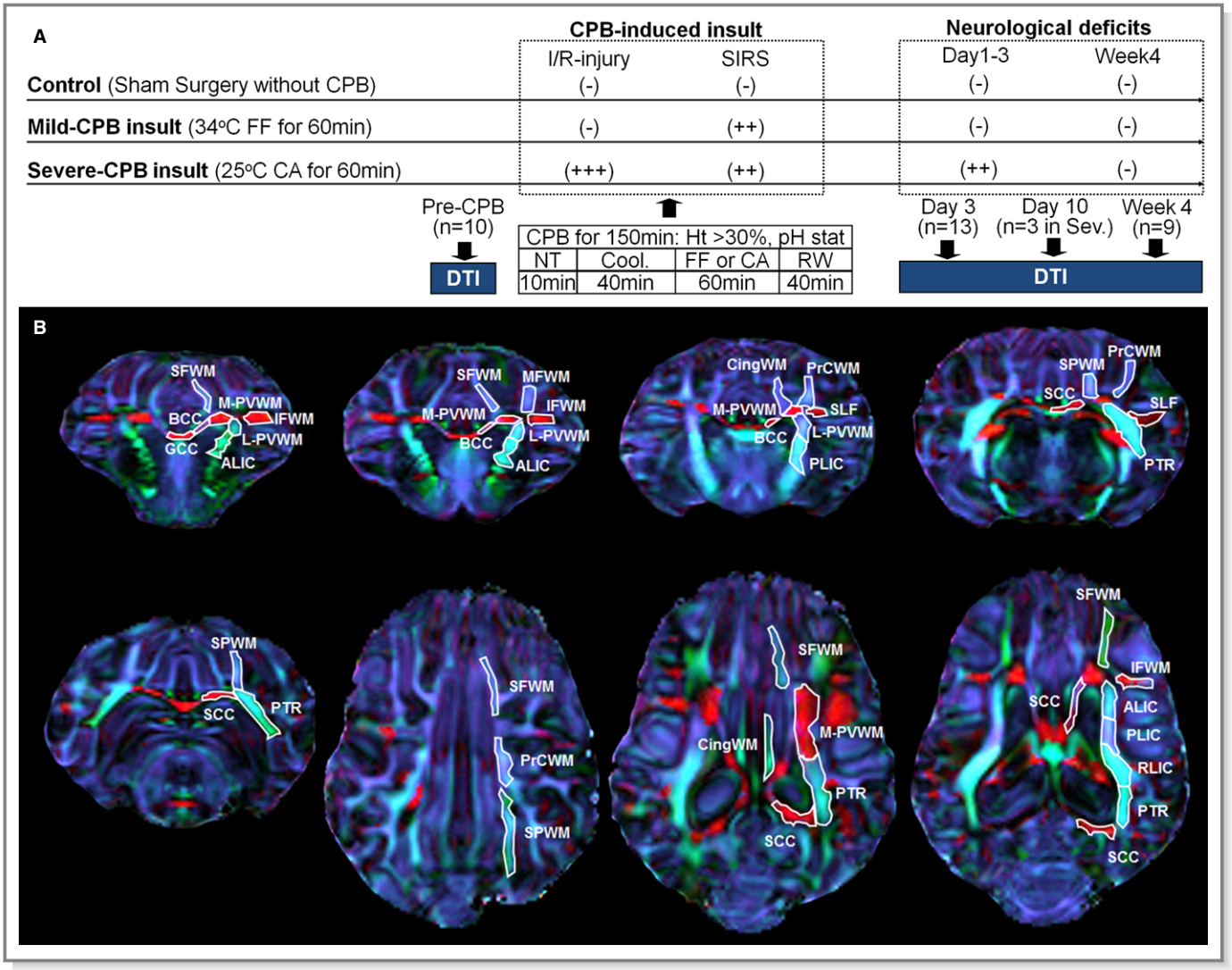

Figure 1. CPB-induced insult and porcine WM structures. A, Study design of the CPB groups. More data are presented in Table 1. B, The anatomical location and example of drawn and quantified region of interests in porcine WM structures on directionally encoded color map. ALIC indicates anterior limb of the internal capsule; BCC, body of the corpus callosum; CA, circulatory arrest; CingWM, cingulum white matter; Cool, cooling; CPB, cardiopulmonary bypass; DTI, diffusion tensor imaging; FF, full-flow perfusion; GCC, genu of the corpus callosum; Ht, hematocrit level; I/R, ischemia-reperfusion/reoxygenation; IFWM, inferior frontal white matter; L-PVWM, lateral periventricular white matter; MFWM, middle frontal white matter; M-PVWM, medial periventricular white matter; NT, normothermia; PLIC, posterior limb of the internal capsule; PrCWM, precentral white matter; PTR, posterior thalamic radiation; RLIC, retrolenticular limb of the internal capsule; RW, rewarming; SCC, splenium of the corpus callosum; Sev., severe-CPB insult; SFWM, superior frontal white matter; SIRS, systemic inflammatory response syndrome; SLF, superior longitudinal fasciculus; SPWM, superior-parietal white matter; WM, white matter.

tube. Each animal was ventilated at an inspired oxygen fraction of 0.21 and a rate of 12 to 15 breaths/min, by means of a volume-control ventilator (Servo Ventilator 300; Siemens, New York, NY) to achieve a normal pH and arterial carbon dioxide tension of 35 to 40 mm Hg. Intravenous bolus injections of fentanyl and pancuronium via a peripheral intravenous line were administered before surgery. Anesthesia was maintained by a continuous infusion of fentanyl, midazolam, and pancuronium throughout the entire experiment. Heterologous blood was obtained from a donor Yorkshire pig with weight of 35 to 45 kg that had been anesthetized with telazol and xylazine. Under anesthesia an intravenous cannula was placed in each femoral vein to obtain the blood. Heparin was administered intravenously. The donated blood was used to prime the CPB circuits for the experimental animals.

Surgery and Cardiopulmonary Bypass

All surgical procedures were performed under sterile conditions. Two cannulas (19G Intracath; Becton Dickinson, Sandy, UT) were inserted in the right femoral artery and vein,

respectively, for continuous blood pressure monitoring and blood sampling and continuous infusion. For the perioperative temperature monitoring, temperature probes were placed in the esophagus and rectum. A right anterolateral thoracotomy was performed through the third intercostal space to expose the ascending aorta for arterial cannulation and the right atrium for venous cannulation, respectively. After systemic heparinization (300 IU/kg) administered intravenously, a 10F arterial cannula (Medtronic Bio-Medics, Minneapolis, MN) and a 22F venous cannula (Research Medical Inc, Midvale, UT) were inserted into the ascending aorta and right atrial appendage, respectively. The CPB circuit consisted of a roller-pump (Cardiovascular Instrument Corp; Wakefield, MA), membrane oxygenator (Minimax; Medtronic Inc, Anaheim, CA), and sterile tubing with 40-μm arterial filter. Fresh whole blood from a donor pig was transfused into the CPB circuit in order to adjust the hematocrit level to 30%.[28-30] The pump prime included normal saline, methylprednisolone (30 mg/kg), furosemide (0.25 mg/kg), sodium carbonate (10 mL), and cephazolin sodium (25 mg/kg). The pH-stat strategy was employed by the use of sweep gas 95% O_2/5% CO_2.[31,32] CPB was started, and the animals were perfused for 10 minutes at an esophageal temperature of 37°C. Subsequently animals were cooled to an esophageal temperature of 25°C or 34°C according to the experimental protocol. Ventilation was stopped after the establishment of CPB. After cooling, circulatory arrest or maintenance of full flow was chosen according to the protocol. Duration of the circulatory arrest period was 60 minutes. During the rewarming period the heart was defibrillated as necessary at an esophageal temperature of 30°C. Ventilation was started 10 minutes before weaning from CPB. After 40 minutes of rewarming, animals were weaned from CPB. The hematocrit level of 30% was maintained, and pH-stat strategy was performed as described in the current clinical CPB technique.[26,29] Mean and systolic arterial pressure and esophageal and rectal temperature were monitored continuously throughout each experiment and were recorded every 10 minutes. Arterial P_{O_2} and P_{CO_2}, arterial pH, hematocrit value, mixed venous oxygen saturation, and arterial lactate were measured with a blood gas analyzer (Rapidlab 1200; Siemens, New York, NY) every 15 minutes on CPB, at 30 minutes after conclusion of CPB, and once an hour up to extubation on postoperative day 1.[33] The tissue oxygen index was measured using near-infrared spectroscopy.[33] Neurological and behavioral evaluations were performed blindly at 24-hour intervals beginning on postoperative day 1. Experimental conditions are described in Table 1.

Diffusion Tensor Imaging

Conventional anatomical T1 and T2 MRI and DTI images were acquired on a GE Signa HDxt 3.0T scanner (GE Medical Systems, Milwaukee, WI) using a GE Quad Knee coil. Prior to DTI measurement, we acquired conventional coronal and axial T2-weighted fast spin-echo T2 fluid attenuation inversion recovery (FLAIR), and T1-weighted FLAIR imaging sequences with the following parameters: axial T1 FLAIR, echo time (TE)=7 ms, recovery time (TR)=3000 ms, inversion recovery time (TIR)=1238ms, echo train length=7, matrix=256×128, 3-mm slice, 2 average; axial T2 fast spin-echo, TE=90 ms, TR=2200 ms, echo train length=25, matrix=256×128, 3-mm slice, 8 average; axial T2 FLAIR, TE=96 ms, TR=6000 ms, TIR=2400 ms, matrix=256×128, 3-mm slice, 2 average; coronal T1 FLAIR, TE=9 ms, TR=3000 ms, TIR=1238 ms, echo train length=7, matrix=320×224, 3-mm slice, 1 average; coronal T2 fast spin-echo, TE=90 ms, TR=4000 ms, echo train length=25, matrix=256×128, 3-mm slice, 8 average; and coronal T2 FLAIR, TE=90 ms, TR=6000 ms, TIR=2400 ms, matrix=256×128, 2-mm slice, 2 average. DTI data were obtained using a single-shot spin echo (SE) echoplanar imaging axial DTI sequence with the following parameters: TE=102.5 ms, TR=6000 ms, matrix=128×128, 4-mm slice, 1 reference plus 15 directions with diffusion weighting (b=1000 s/mm^2) with 8 average. All animals were sedated with intramuscular ketamine and xylazine before imaging. Anesthesia was maintained by isoflurane. Intravenous fluid was administered via the venous line during entire imaging experiment. The status of anesthesia and hemodynamics was continuously monitored by an MRI-compatible monitoring system (Invivo Co, Orlando, FL). The MR images were transferred offline and reviewed by an MR physicist and a neuroradiologist. We performed a total of 40 MRI studies (pre-CPB, n=13; post-CPB day 3, n=13; post-CPB day 10, n=4; post-CPB day 17, n=1; week 4, n=9). Within a total of 40 imaging experiments, 5 experiments were excluded from our analysis (inadequate image quality n=4, different time point for preliminary analysis n=1). Among 35 imaging studies analyzed, a total of 10 experiments were performed preoperatively (Figure 1A). We also analyzed 13 and 9 imaging studies on post-operative day 3 (control n=3, mild-CPB n=4, and severe-CPB n=6) and week 4 (control n=3, mild-CPB n=3, severe-CPB n=3), respectively (Figure 1A). To assess normal FA changes in porcine WM, data obtained from preoperative studies (3 weeks of age; n=10) as well as in controls on postoperative week 4 (7 weeks of age, n=3) were analyzed. Three additional MRI imaging studies were performed on postoperative day 10 to define changes of FA after severe-CPB (Figure 1A). DTI data were processed using GE FuncTool software (Waukesha, WI). To avoid issues associated with spatial normalization of WM tracts, we applied a region-of-interest (ROI) approach to test specific structures throughout the brain selected in an a priori knowledge fashion. Free-form polygon ROIs were identified using anatomical images and directionally encoded color FA maps. All ROIs were drawn

Table 1. Experimental Conditions

CPB Groups	Control (n=3)		Mild CPB (n=4)		Severe CPB (n=6)		F-Test	*P* Value	Control vs Mild CPB	Control vs Severe CPB	Mild CPB vs Severe CPB
	Mean	SD	Mean	SD	Mean	SD					
Body weight, kg	5.0	0.8	4.6	0.9	4.8	0.8	0.17	0.844			
Tissue oxygen index											
Pre-CPB	50.0	4.4	45.1	2.8	48.1	2.6	2.24	0.157			
Pre-FF/CA	50.7	3.8	56.6	1.3	66.7	4.2	23.49	<0.001	0.158	<0.001	0.004
FF/CA	53.3	4.3	57.0	1.3	34.0	2.9	87.01	<0.001	0.384	<0.001	<0.001
Post-FF/CA	50.6	5.3	52.4	2.0	52.4	1.6	0.46	0.643			
Post-CPB	51.2	5.0	49.7	2.4	47.2	2.0	2.09	0.175			
Mean blood pressure, mm Hg											
Pre-CPB	88.2	3.3	76.6	17.7	79.6	20.7	0.39	0.689			
Pre-FF/CA	88.4	3.3	96.0	6.0	101.3	4.7	6.92	0.013	0.213	0.012	0.379
FF/CA	87.1	5.0	99.1	7.4	4.8	1.7	568.20	<0.001	0.024	<0.001	<0.001
Post-FF/CA	86.7	5.6	112.7	11.8	111.6	20.4	2.91	0.101			
Post-CPB	83.4	4.6	92.9	15.7	82.4	7.6	1.35	0.302			
Esophageal temperature, °C											
Pre-CPB	36.6	1.1	36.3	1.2	36.3	1.2	0.05	0.951			
Pre-FF/CA	36.7	1.2	34.6	0.3	28.9	1.1	76.50	<0.001	0.050	<0.001	<0.001
FF/CA	36.9	1.2	33.6	0.7	25.0	1.1	172.10	<0.001	0.004	<0.001	<0.001
Post-FF/CA	37.0	1.3	36.9	0.6	36.5	1.1	0.32	0.732			
Post-CPB	36.9	1.3	37.8	0.5	37.3	0.8	1.18	0.347			
Pa_{O_2}, mm Hg											
Pre-CPB	101.5	11.3	108.0	6.6	98.0	11.0	1.20	0.341			
Pre-FF/CA	94.5	13.4	548.8	46.3	574.8	42.5	161.50	<0.001	<0.001	<0.001	0.999
Post-FF/CA	93.3	11.8	549.5	28.1	503.9	35.6	239.00	<0.001	<0.001	<0.001	0.121
Post-CPB	95.5	10.2	121.9	27.9	122.7	25.9	1.42	0.287			
Pa_{CO_2}, mm Hg											
Pre-CPB	33.2	12.5	31.4	1.4	31.5	9.2	0.05	0.955			
Pre-FF/CA	35.4	9.5	40.7	3.1	42.7	3.5	1.99	0.187			
Post-FF/CA	38.1	5.5	39.7	1.4	39.9	4.3	0.21	0.812			
Post-CPB	37.1	5.1	32.1	5.1	31.3	5.6	1.25	0.327			
PH											
Pre-CPB	7.64	0.09	7.67	0.10	7.62	0.10	0.30	0.745			
Pre-FF/CA	7.60	0.04	7.51	0.04	7.46	0.04	11.40	0.003	0.061	0.002	0.234
Post-FF/CA	7.56	0.03	7.54	0.04	7.43	0.02	25.40	<0.001	0.999	<0.001	0.001
Post-CPB	7.55	0.04	7.61	0.07	7.57	0.09	0.61	0.563			
Hematocrit, %											
Pre-CPB	37.2	2.4	37.1	3.6	38.4	2.4	0.34	0.721			
Pre-FF/CA	36.7	2.3	34.3	2.0	34.2	2.7	1.13	0.361			
Post-FF/CA	36.3	1.6	33.5	1.4	33.9	2.5	1.85	0.208			
Post-CPB	36.6	3.4	36.9	1.6	34.5	3.0	1.11	0.367			

Continued

Table 1. Continued

CPB Groups	Control (n=3)		Mild CPB (n=4)		Severe CPB (n=6)		F-Test	*P* Value	Control vs Mild CPB	Control vs Severe CPB	Mild CPB vs Severe CPB
	Mean	SD	Mean	SD	Mean	SD					
Leukocyte number, $\times 10^3/\mu L$											
Pre-CPB	5.8	0.4	5.5	1.6	6.4	1.8	0.38	0.691			
Pre-FF/CA	6.3	2.2	6.6	2.0	4.4	1.1	0.38	0.691			
Post-FF/CA	6.9	2.6	7.2	1.8	7.6	2.7	0.07	0.929			
Post-CPB	7.6	1.8	15.7	4.5	15.5	4.0	5.00	0.031	0.061	0.046	0.999
Blood lactate concentration, mmol/L											
Pre-CPB	1.4	0.4	1.3	0.5	1.6	0.4	0.50	0.618			
Pre-FF/CA	1.5	0.5	2.2	1.0	2.7	0.5	3.03	0.094			
Post-FF/CA	1.9	1.1	1.3	0.8	6.6	1.6	23.24	<0.001	0.999	0.002	0.000
Post-CPB	2.2	1.0	1.4	0.7	5.0	1.4	12.76	0.002	0.999	0.022	0.002
Total NDS (day 1-3)	0.0	0.0	35.0	30.0	280.8	74.4	36.53	<0.001	0.999	<0.001	<0.001
Total OPC (day 1-3)	3.0	0.0	4.0	1.2	7.8	1.0	34.19	<0.001	0.581	<0.001	<0.001

CA indicates circulatory arrest; CPB, cardiopulmonary bypass; FF, full-flow perfusion; NDS, neuronal deficit score; OPC, overall performance category; $Paco_2$, partial pressure of carbon dioxide; Pao_2, partial pressure of oxygen.

and quantified manually using MIPAV freeware (NIH, Bethesda, MD). The anatomical locations of ROIs are described in the directionally encoded color map using ex vivo imaging methods in Figure 1B. Brains in the skull were isolated by removal at the first vertebra and removing the jaw up to the soft palate. Skulls were then incubated in 4% paraformaldehyde overnight followed by 1 week in 1% paraformaldehyde followed by 2 weeks in PBS all on a rocker at 4°C. Skulls were taken out and allowed to come to room temperature for at least 6 hours before imaging. The images were acquired on a Bruker BioSpin 7.0T scanner (Bruker BioSpin Corporation, Billerica, MA) in a Bruker 72-mm volume coil. Two DTI echoplanar imaging scans were acquired with a TE=34.44 ms, and TR=700 ms. A total of 30 diffusion sampling directions were acquired along with 5 images with 0 diffusion (b=2500 s/mm^2). Images were acquired in 3 dimensions with an isotropic voxel size of 0.5078 mm per side. A structural multiecho TurboRare T2 image with a TR of

Table 2. Distinguished Porcine White Matter Structures

Abbreviation	Structure	Deep/Superficial White Matter	Fiber Category	Subdivision
GCC	Genu of corpus callosum	Deep white matter	Commissural	Corpus callosum
BCC	Body of corpus callosum	Deep white matter	Commissural	Corpus callosum
SCC	Splenium of corpus callosum	Deep white matter	Commissural	Corpus callosum
ALIC	Anterior limb of internal capsule	Deep white matter	Projection	Internal capsule
PLIC	Posterior limb of internal capsule	Deep white matter	Projection	Internal capsule
RLIC	Retrolenticular part of internal capsule	Deep white matter	Projection	Internal capsule
M-PVWM	Medial periventricular white matter (superior corona radiata)	Deep white matter	Projection	Distant projection
L-PVWM	Lateral periventricular white matter (superior corona radiata)	Deep white matter	Projection	Distant projection
PTR	Posterior thalamic radiation	Deep white matter	Projection	Distant projection
SLF	Superior longitudinal fasciculus	Deep white matter	Association	Deep white matter association
CingWM	Cingulum white matter	Deep white matter	Association	Deep white matter association
SFWM	Superior frontal white matter	Superficial white matter	Association	Frontal superficial white matter
MFWM	Middle frontal white matter	Superficial white matter	Association	Frontal superficial white matter
IFWM	Inferior frontal white matter	Superficial white matter	Association	Frontal superficial white matter
PrCWM	Precentral white matter	Superficial white matter	Association	Parietal superficial white matter
SPWM	Superior parietal white matter	Superficial white matter	Association	Parietal superficial white matter

Table 3. White Matter ROI Volumes

	Pre-CPB (n=10)			Day 3 (n=13)			Week 4 (n=9)		
WM Regions	Mean	SD	%CV	Mean	SD	%CV	Mean	SD	%CV
GCC	7.111	1.942	27.305	7.225	1.416	19.596	7.349	2.108	28.684
BCC	5.187	0.566	10.916	5.100	1.270	24.900	5.711	1.472	25.765
SCC	7.826	1.609	20.557	7.939	1.138	14.332	8.540	1.929	22.587
ALIC	12.321	3.174	25.759	12.363	2.549	20.616	12.816	2.105	16.427
PLIC	19.064	3.129	16.412	18.346	3.194	17.413	21.331	3.198	14.994
RLIC	16.064	3.645	21.337	14.446	3.428	25.232	18.613	3.023	16.243
M-PVWM	4.214	1.126	26.732	4.121	0.914	22.180	4.313	1.096	25.411
L-PVWM	6.588	0.977	27.756	7.445	1.829	37.700	6.830	2.807	28.424
PTR	13.770	3.316	24.085	13.593	2.736	20.130	16.431	3.473	21.135
SLF	9.554	2.570	26.895	8.832	0.930	10.535	10.116	1.813	17.925
CingWM	8.404	1.738	20.682	8.462	2.652	31.342	10.033	1.795	17.894
SFWM	13.375	2.134	15.957	13.164	1.672	12.700	14.005	2.871	20.497
MFWM	12.684	1.382	10.897	14.055	2.411	17.153	15.434	3.005	19.472
IFWM	9.397	2.551	27.148	10.076	1.620	16.074	11.145	2.050	18.391
PrCWM	8.344	1.240	14.864	7.791	1.243	15.955	10.163	3.294	32.417
SPWM	8.979	2.829	31.506	8.271	1.695	20.497	10.177	1.915	18.822

ALIC indicates anterior limb of the internal capsule; BCC, body of the corpus callosum; CingWM, cingulum white matter; CPB, cardiopulmonary bypass; CV, coefficient of variation; FA, fractional anisotropy; GCC, genu of the corpus callosum; IFWM, inferior frontal white matter; L-PVWM, lateral periventricular white matter; MFWM, middle frontal white matter; M-PVWM, medial periventricular white matter; PLIC, posterior limb of the internal capsule; PrCWM, precentral white matter; PTR, posterior thalamic radiation; RLIC, retrolenticular limb of the internal capsule; ROI, region of interest; SCC, splenium of the corpus callosum; SFWM, superior frontal white matter; SLF, superior longitudinal fasciculus; SPWM, superior-parietal white matter; WM, white matter.

700 and TEs of 34, 124.66, 215.33, and 305.99 ms, rare factor of 8, and 2 averages was also acquired. Tolerably Obsessive Registration and Tensor Optimization Indolent Software Ensemble (TORTOISE) was used to account for echoplanar imaging and eddy current distortion and to process directionally encoded color maps.[34] A total of 31 WM structures in a porcine brain (Table 2) were constructed based on the DTI-based human brain WM (DTI studio: Susumu Mori, Johns Hopkins University).[35] Within a total of 88 human WM structures, superior corona radiata was subdivided into medial periventricular white matter (M-PVWM) and lateral periventricular white matter (L-PVWM) because of the significant developmental differences obtained from our previous immunohistochemistrical analysis using the porcine developmental model (Table 2).[22] Each structure was further categorized based on (1) the deep or superficial WM, (2) type of fiber, and (3) 6 subdivisions (Table 2). FA is a scalar value between 0 and 1 that describes the degree of anisotropy of water diffusion processes in tissues.[14] An FA value of 0 means that water diffusion is isotropic, ie, is unrestricted (or equally restricted) in all directions, whereas an FA value of 1 means water diffusion is unidirectional.[14] WM volume in each distinct follow-up group confirmed the minimum variation of drawn ROI volumes (Table 3), demonstrating the reliability of our FA measurement. Two observers blindly measured FA in 16 analyzed WM structures. The intraobserver correlation indicated strong agreement (Figure 2A).

Immunohistochemistry

Before being postfixed for an additional 24 hours at 4°C in 4% paraformaldehyde, the brain was separated into sections. The sections were soaked for 24 hours in 15% sucrose in phosphate-buffered saline, pH 7.4, followed by 48 hours in 30% sucrose in phosphate-buffered saline, pH 7.4. All samples were embedded in OCT compound, sliced with a cryostat at −20°C, and stored at −80°C until immunohistochemical processing. Twenty-micrometer sections were incubated for 1 hour at room temperature with blocking solution (20% normal goat serum, 1% bovine serum albumin, and 0.3% Tween 20 in phosphate-buffered saline, pH 7.4) and then incubated at 4°C overnight with primary antibody and carrier solution (2% normal goat serum, 2% bovine serum albumin, and 0.3% Tween 20 in phosphate-buffered saline, pH 7.4). Species-specific secondary fluorescent antibodies (1:200; Jackson ImmunoResearch Laboratories, Inc, West Grove, PA) were diluted in carrier solution and applied to sections for 1 hour at room temperature. Sections were mounted with

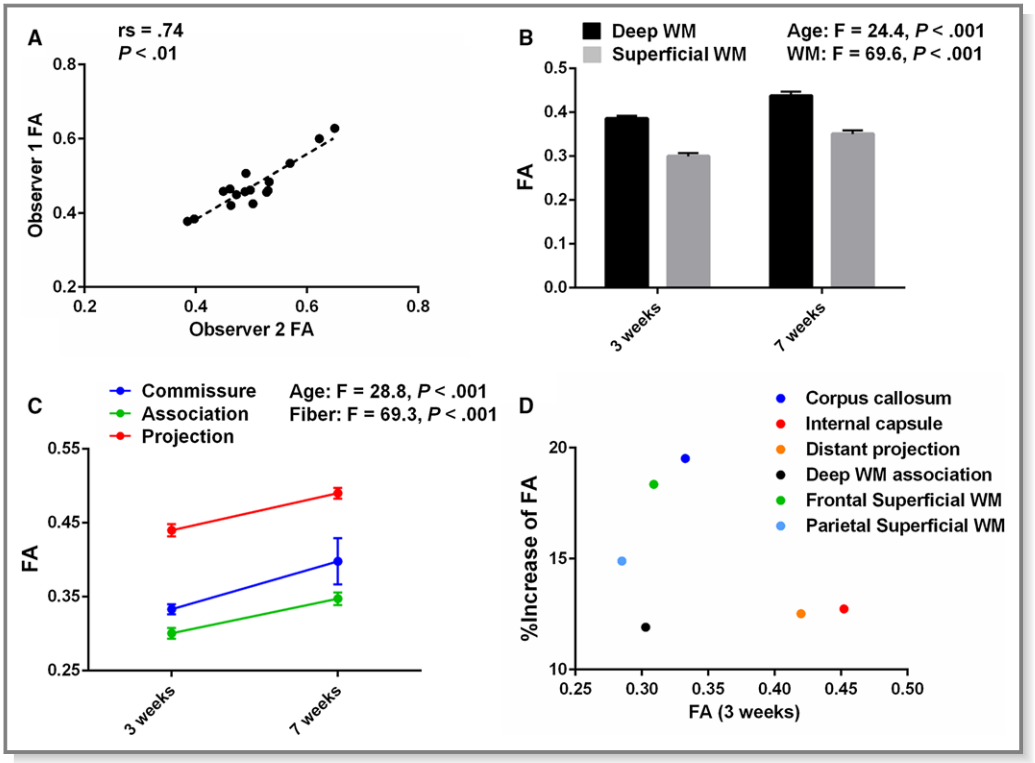

Figure 2. The piglet brain is a powerful model to study human white matter (WM) development. A, Intraobserver correlation of FA analyzed using ROI measurements from diffusion tensor images by the Spearman rank-order correlation coefficient (16 WM structures analyzed). B, FA in the deep WM of the pig is significantly higher than in superficial WM at 3 and 7 weeks of age, as observed in human WM (3 weeks, n=10; 7 weeks, n=3). More data are presented in Table 4. C, Consistent with findings in human WM development, FA in porcine WM is highest in projection fibers and lowest in association fibers at each age (3 weeks, n=10 in each; 7 weeks, n=3 in each). More data are presented in Table 4. D, Plot of FA in 6 porcine WM subregions at 3 weeks of age, and the change from 3 to 7 weeks demonstrates a structure-specific maturation pattern similar to human WM development (3 weeks, n=10 in each; 7 weeks, n=3 in each). More data are presented in Table 4. FA indicates fractional anisotropy; ROI, region of interest.

VECTASHIELD mounting medium for fluorescence with 4′,6-diamidino-2-phenylindole (Vector Laboratories, Inc, Burlingame, CA). The following antibodies were used for immunohistochemistry: anti-Olig2 (1:1000; Millipore, Billerica, MA), anti-CC1 (1:1000; Millipore), anti-Glial Fibrillary Acidic Protein (GFAP) (1:1000; DAKO, Santa Clara, CA), anti-Glutamine Synthetase (GS) (1:1000; Millipore), and anti-Iba1 (1:1000; Wako Chemicals, Richmond, VA). Cellular analysis was performed in the coronal section including 7 WM regions: (1) body of corpus callosum (BCC); (2) medial-periventricular WM (M-PVWM); (3) lateral-periventricular WM (L-PVWM); (4) anterior limb of internal capsule; (5) superior frontal WM (SFWM); (6) middle frontal WM (MFWM); and (7) inferior frontal WM (IFWM). Porcine oligodendrocyte lineage cells and mature oligodendrocyte were identified by antibodies to Olig2 and CC1.[36,37] An Iba1 antibody was used to identify microglia. Astrocytes were determined by antibodies to GFAP and GS. Images were acquired on a Zeiss LSM 510 confocal microscope (Carl Zeiss Microimaging LLC, Thornwood, NY). A stereology microscope (Stereo Investigator, MBF Bioscience, Williston, VT) was used to define antibody-positive cell density. The Stereo Investigator system provides systematic random sampling to obtain unbiased estimates of cell number.[38]

Statistical Analysis

The Kolmogorov-Smirnov goodness-of-fit test of normality was performed to assess whether variables followed a normal (Gaussian-shaped) distribution. The Student t test was performed to compare FA values between 3 and 7 weeks of age in normal development and 2 CPB conditions after surgery. We used one-way analysis of variance (ANOVA) with Bonferroni post hoc comparisons to compare perioperative variables and FA in each WM ROI among 3 CPB conditions. Two-way ANOVA with Bonferroni comparisons with WM ROIs treated as a factor was performed to evaluate changes in FA and cell number for WM regions among 3 CPB groups. We applied 2-way ANOVA with Bonferroni post hoc comparisons with time as a factor to evaluate (1) changes in FA under

Table 4. Comparison of Fractional Anisotropy Between Age Groups Stratified by WM Region

	3 Weeks		7 Weeks		
	Mean	SD	Mean	SD	*P* Value
Deep WM	n=10		n=3		
GCC	0.314	0.048	0.406	0.091	0.025*
BCC					
Mean	0.365	0.046	0.407	0.010	0.148
Left	0.380	0.055	0.421	0.044	0.256
Right	0.349	0.047	0.393	0.030	0.147
SCC					
Mean	0.320	0.037	0.380	0.067	0.049*
Left	0.313	0.038	0.395	0.051	0.008*
Right	0.327	0.041	0.365	0.083	0.258
ALIC					
Mean	0.415	0.032	0.511	0.040	<0.001*
Left	0.413	0.036	0.494	0.035	0.004*
Right	0.418	0.035	0.528	0.045	<0.001*
PLIC					
Mean	0.458	0.040	0.517	0.024	0.031*
Left	0.452	0.039	0.525	0.034	0.012*
Right	0.464	0.046	0.509	0.014	0.129
RLIC					
Mean	0.505	0.044	0.495	0.046	0.717
Left	0.483	0.065	0.502	0.048	0.651
Right	0.528	0.035	0.488	0.048	0.124
M-PVWM					
Mean	0.375	0.033	0.428	0.010	0.019*
Left	0.378	0.037	0.454	0.030	0.006*
Right	0.371	0.037	0.403	0.014	0.179
L-PVWM					
Mean	0.439	0.043	0.479	0.009	0.140
Left	0.437	0.049	0.487	0.011	0.112
Right	0.441	0.048	0.472	0.027	0.312
PTR					
Mean	0.445	0.039	0.509	0.010	0.016*
Left	0.421	0.038	0.493	0.026	0.009*
Right	0.470	0.048	0.526	0.019	0.072
SLF					
Mean	0.303	0.033	0.325	0.025	0.326
Left	0.309	0.033	0.326	0.037	0.473
Right	0.297	0.038	0.323	0.014	0.278
CingWM					
Mean	0.302	0.032	0.353	0.013	0.022*
Left	0.285	0.038	0.342	0.013	0.027*
Right	0.319	0.036	0.364	0.027	0.065
Superficial WM	n=10		n=3		
SFWM					
Mean	0.300	0.022	0.342	0.017	0.009*
Left	0.299	0.022	0.343	0.022	0.009*
Right	0.300	0.024	0.341	0.012	0.014*
MFWM					
Mean	0.288	0.045	0.354	0.021	0.032*
Left	0.311	0.053	0.368	0.026	0.103
Right	0.264	0.062	0.340	0.022	0.063
IFWM					
Mean	0.339	0.034	0.401	0.006	0.009*
Left	0.351	0.034	0.398	0.016	0.041*
Right	0.327	0.045	0.404	0.010	0.013*
PrCWM					
Mean	0.305	0.037	0.339	0.032	0.161
Left	0.310	0.040	0.357	0.035	0.092*
Right	0.299	0.040	0.321	0.031	0.038*
SPWM					
Mean	0.265	0.031	0.316	0.013	0.018*
Left	0.256	0.030	0.312	0.030	0.013*
Right	0.275	0.039	0.320	0.026	0.088

FA values are significantly different among WM regions analyzed ($F=34.5$, $P<0.001$) and at ages 3 weeks vs 7 weeks ($F=72.4$, $P<0.001$) by 2-way ANOVA. ALIC indicates anterior limb of the internal capsule; BCC, body of the corpus callosum; CingWM, cingulum white matter; FA, fractional anisotropy; GCC, genu of the corpus callosum; IFWM, inferior frontal white matter; L-PVWM, lateral periventricular white matter; MFWM, middle frontal white matter; M-PVWM, medial periventricular white matter; PLIC, posterior limb of the internal capsule; PrCWM, pre-central white matter; PTR, posterior thalamic radiation; RLIC, retrolenticular limb of the internal capsule; SCC, splenium of the corpus callosum; SFWM, superior frontal white matter; SLF, superior longitudinal fasciculus; SPWM, superior-parietal white matter; WM, white matter.
*$P<0.05$.

normal physiological development and (2) changes in cell number after severe CPB between WM ROIs. Factorial 2-way ANOVA (rather than repeated-measures ANOVA) was applied for the assessment because of the exclusion of some imaging data due to the inadequate quality and factorial experimental design in the cellular assay. To determine the association of cellular events on changes of FA for each WM ROI, we first applied linear regression methods and analyzed the relationships separately for each distinct group. Linear trend between 2 groups was tested in the model. Relationships between FA values and antibody-positive cell numbers were analyzed using nonparametric tests including the Mann-Whitney U-test,

Table 5. Fractional Anisotropy in Each WM Region on Postoperative Day 3 and Week 4

CPB Groups	Control		Mild CPB		Severe CPB		F Test	*P* Value	Control vs Mild CPB	Control vs Severe CPB	Mild CPB vs Severe CPB
WM Regions	Mean	SD	Mean	SD	Mean	SD					
Day 3*	n=3		n=4		n=6						
GCC	0.291	0.025	0.315	0.078	0.350	0.037	1.458	0.272			
BCC	0.370	0.037	0.380	0.036	0.372	0.025	0.116	0.892			
SCC	0.291	0.030	0.327	0.032	0.327	0.029	1.615	0.247			
ALIC	0.426	0.015	0.439	0.042	0.440	0.047	0.131	0.879			
PLIC	0.473	0.010	0.475	0.056	0.469	0.026	0.111	0.896			
RLIC	0.530	0.036	0.442	0.102	0.489	0.026	1.830	0.210			
M-PVWM	0.375	0.035	0.385	0.035	0.427	0.035	2.882	0.103			
L-PVWM	0.449	0.039	0.456	0.048	0.461	0.029	0.104	0.903			
PTR	0.437	0.016	0.432	0.041	0.458	0.029	0.979	0.409			
SLF	0.315	0.038	0.298	0.031	0.301	0.032	0.238	0.793			
CingWM	0.282	0.021	0.299	0.018	0.319	0.030	2.318	0.149			
SFWM	0.303	0.021	0.303	0.031	0.316	0.041	0.231	0.798			
MFWM	0.303	0.037	0.295	0.050	0.271	0.060	0.465	0.641			
IFWM	0.360	0.031	0.337	0.026	0.331	0.062	0.363	0.704			
PrCWM	0.339	0.005	0.307	0.046	0.283	0.015	4.101	0.050	0.157	0.017	0.219
SPWM	0.260	0.006	0.260	0.051	0.279	0.039	0.393	0.685			
Week 4†	n=3		n=3		n=3						
GCC	0.406	0.091	0.424	0.026	0.260	0.023	7.741	0.022	0.705	0.019	0.012
BCC	0.407	0.010	0.451	0.038	0.343	0.029	11.249	0.009	0.106	0.031	0.003
SCC	0.380	0.067	0.373	0.047	0.331	0.040	0.770	0.504			
ALIC	0.511	0.040	0.478	0.028	0.482	0.022	1.019	0.416			
PLIC	0.517	0.024	0.516	0.003	0.510	0.025	0.117	0.891			
RLIC	0.495	0.046	0.553	0.003	0.518	0.057	1.439	0.309			
M-PVWM	0.428	0.010	0.404	0.033	0.412	0.086	0.160	0.855			
L-PVWM	0.479	0.009	0.513	0.026	0.496	0.015	2.669	0.148			
PTR	0.509	0.010	0.482	0.023	0.485	0.061	0.464	0.650			
SLF	0.325	0.025	0.310	0.016	0.311	0.038	0.244	0.791			
CingWM	0.353	0.013	0.312	0.041	0.330	0.036	1.229	0.357			
SFWM	0.342	0.017	0.374	0.005	0.319	0.008	17.712	0.003	0.014	0.045	0.001
MFWM	0.354	0.021	0.325	0.017	0.286	0.024	7.971	0.020	0.136	0.007	0.065
IFWM	0.401	0.006	0.298	0.008	0.353	0.084	3.352	0.105			
PrCWM	0.339	0.032	0.308	0.011	0.315	0.017	1.645	0.269			
SPWM	0.316	0.013	0.342	0.001	0.309	0.021	4.562	0.062			

ALIC indicates anterior limb of the internal capsule; BCC, body of the corpus callosum; CingWM, cingulum white matter; CPB, cardiopulmonary bypass; FA, fractional anisotropy; GCC, genu of the corpus callosum; IFWM, inferior frontal white matter; L-PVWM, lateral periventricular white matter; MFWM, middle frontal white matter; M-PVWM, medial periventricular white matter; PLIC, posterior limb of the internal capsule; PrCWM, precentral white matter; PTR, posterior thalamic radiation; RLIC, retrolenticular limb of the internal capsule; SCC, splenium of the corpus callosum; SFWM, superior frontal white matter; SLF, superior longitudinal fasciculus; SPWM, superior parietal white matter; WM, white matter.

*FA values are significantly different among 16 WM regions ($F=41.2$, $P<0.001$), but not between CPB groups ($F=1.06$, $P=0.348$) by 2-way ANOVA.

†FA values are significantly different among 16 WM regions ($F=44.5$, $P<0.001$) and between CPB groups ($F=10.8$, $P<0.001$) by 2-way ANOVA. There are significant interactions between WM regions and CPB ($F=2.39$, $P<0.001$).

Kruskal-Wallis H-test with multiple-comparison procedure[39] and the Spearman rank-order correlation coefficient (r_s). Previous studies demonstrated that cellular maturation in the human WM involves expansion of oligodendrocyte lineages and axonal myelination by mature oligodendrocytes followed by a decline of mature oligodendrocytes.[37,40,41] Based on

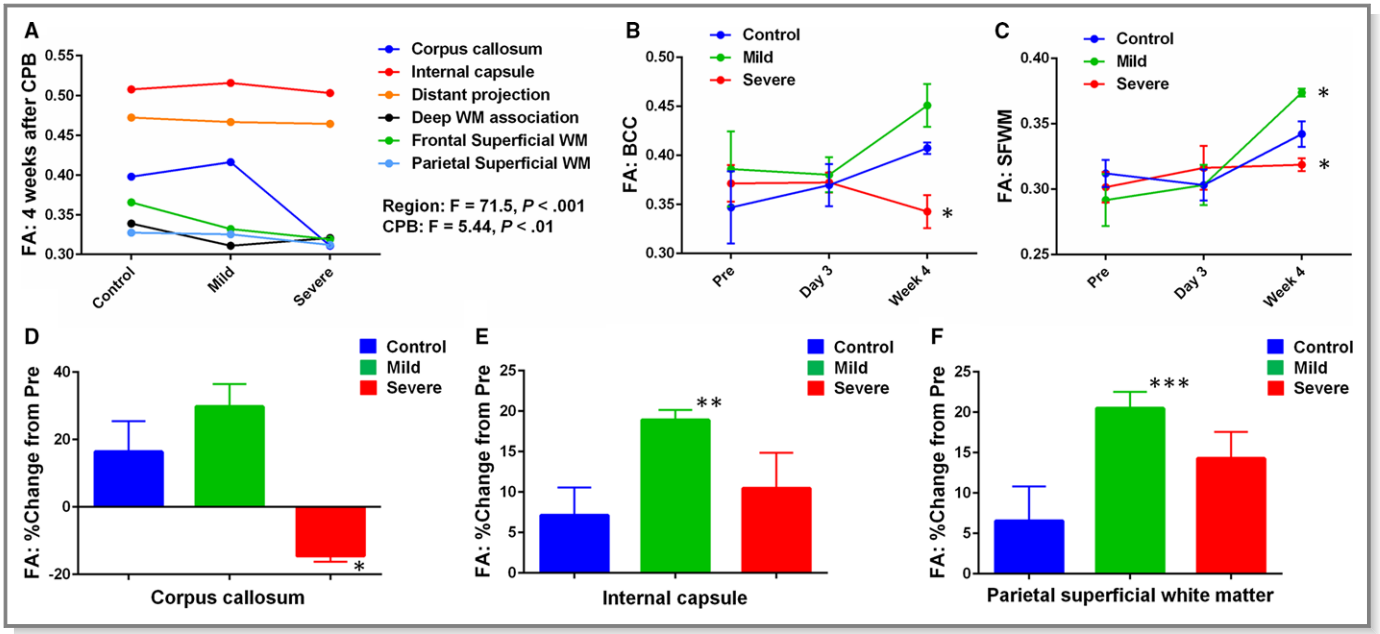

Figure 3. There is maturation-dependent WM vulnerability following CPB. FA changes after CPB are also insult-dependent. A, The decrease in FA after severe CPB is identified in the corpus callosum and the frontal superior WM, where the largest FA change from 3 to 7 weeks is observed in normal WM development (Figure 2D). FA in internal capsule and distant projection, which are characterized as mature WM regions with high FA and low changes (Figure 2D), demonstrates no changes following CPB, indicating maturation-dependent WM vulnerability to insults associated with congenital heart surgery (n=3 in each). More data are presented in Table 5. B and C, Although there are no changes in FA on post-CPB day 3, severe CPB results in significant FA decreases in BCC (B) and SFWM (C) 4 weeks postoperatively. A significant FA increase is also seen in SFWM (C) following mild CPB (n=3-6 in each). More data are presented in Table 5. D through F, Percentage change of FA from preoperation displays a significant decrease in FA after severe CPB in the corpus callosum (D); on the other hand, mild CPB causes FA increase in the internal capsule and parietal superficial WM compared with control (E and F), demonstrating insult-dependent FA alterations after cardiac surgery (n=3 in each). More data are presented in Table 8. **P*<0.05 vs other CPB groups by ANOVA with Bonferoni comparison, ***P*<0.05, ****P*<0.01 vs control by Student t test. Data are shown as mean±SEM. BCC indicates body of the corpus callosum; CPB, cardiopulmonary bypass; FA, fractional anisotropy. Pre, preoperation; SFWM, superior frontal white matter; WM, white matter.

previous evidence regarding cellular processes underlying WM maturation, a Gaussian equation (Gauss-Newton) was applied to nonlinear regression model in control WM and was based on ordinary least squares for minimizing the sum of the squared residuals to derive the best-fitting curve to the data.[42] Nonlinear regression weighted each point equally in describing the curvilinear relationship between Olig2-positive cells and FA. Our nonlinear method aimed to reduce the sum of the squared errors by assuming that the least-squares function was locally quadratic and then finding the minimum of the quadratic curve (ie, the objective function is approximately quadratic). Because the model was applied to all data at 7 weeks of age (ie, no range of time points), thresholds of the range were not determined for the fitted regression model. With the nonlinear regression method, fit statistics and R^2 values between FA values and Olig2-positive cell numbers were estimated. To ascertain the effects of mature oligodendrocyte and microglia cell numbers on FA reduction, we used logistic regression analysis in which we examined cutoff values and defined the binary outcomes as a reduction of 1 SD below the mean FA for the controls for each WM structure. Receiver-operating characteristic curve analysis with the Youden J-index was applied to ascertain the predictive accuracy between CPB-induced FA reduction and change in number of mature oligodendrocytes relative to control. Probability curves were derived by maximum-likelihood estimation in logistic regression to illustrate FA reduction as a function of the changes in oligodendrocytes and microglia number relative to control on post-CPB. Statistical analysis was performed using the PRISM6 software package (GraphPad Software, Inc, La Jolla, CA) and IBM SPSS Statistics Version 23.0 (IBM Corporation, Armonk, NY).

Results

The Structure-Specific Maturation Pattern in the Porcine Model Is Similar to Human WM Development, and WM Development in the Postnatal Porcine Brain Represents Early Infancy in Human WM

In our porcine developmental model, FA values were significantly different among tested WM structures

Table 6. FA in Each WM Subregion on Postoperative Day 3 and Week 4

	Control		Mild CPB		Severe CPB		F Test	*P* Value	Control vs Mild CPB	Control vs Severe CPB	Mild CPB vs Severe CPB
	Mean	SD	Mean	SD	Mean	SD					
Day 3*	n=3		n=4		n=6						
Corpus callosum	0.3170	0.0198	0.3405	0.0470	0.3498	0.0106	1.348	0.3031			
Internal capsule	0.4762	0.0179	0.4521	0.0559	0.4663	0.0236	0.410	0.6745			
Distant projection	0.4203	0.0056	0.4243	0.0366	0.4488	0.0233	1.648	0.2407			
Deep WM association	0.2984	0.0187	0.2987	0.0099	0.3101	0.0263	0.476	0.6345			
Frontal superior WM	0.3221	0.0248	0.3117	0.0343	0.3062	0.0459	0.166	0.8492			
Parietal superior WM	0.2994	0.0053	0.2834	0.0486	0.2813	0.0205	0.377	0.6956			
Week 4†	n=3		n=3		n=3						
Corpus callosum	0.3977	0.0539	0.4162	0.0370	0.3110	0.0109	6.469	0.0318	0.5755	0.0321	0.0151
Internal capsule	0.5075	0.0282	0.5158	0.0094	0.5030	0.0345	0.183	0.8374			
Distant projection	0.4723	0.0032	0.4666	0.0275	0.4643	0.0532	0.043	0.9584			
Deep WM association	0.3389	0.0186	0.3110	0.0290	0.3208	0.0365	0.716	0.5260			
Frontal superior WM	0.3656	0.0138	0.3321	0.0066	0.3191	0.0379	3.095	0.1193			
Parietal superior WM	0.3274	0.0131	0.3254	0.0055	0.3119	0.0090	2.255	0.1861			

CPB indicates cardiopulmonary bypass; FA, fractional anisotropy; WM, white matter.
*FA values are significantly different among 6 WM subregions ($F=69.3$, $P<0.001$) but not among 3 CPB groups ($F=0.58$, $P=0.564$) by 2-way ANOVA.
†FA values are significantly different among 6 WM subregions ($F=71.5$, $P<0.001$) and among 3 CPB groups ($F=5.44$, $P<0.01$) by 2-way ANOVA.

($F=34.5$, $P<0.001$) and at ages 3 weeks versus 7 weeks ($F=72.4$, $P<0.001$). The means and standard deviations for each structure in 2 age groups are given in Table 4. FA in the deep WM was significantly higher than those in superficial WM in both age groups (Figure 2B). Within 3 fiber categories consisting of commissural, projection, and association fibers, FA was highest in projection fibers and lowest in association fibers at each age (Figure 2C). These observations are consistent with findings in a structure-specific maturation pattern to human WM development.[43-45] The porcine WM showed asymmetric diffusion properties at each age group, and the developmental pattern was also asymmetric (Table 4). FA asymmetry and hemispheric lateralization have been widely observed in the human brain and are important in neurological function.[43,46] When we plot FA values at postnatal 3 weeks and the changes from 3 to 7 weeks, corpus callosum (CC) has the largest FA change (19.5%) among 6 representative WM regions (Figure 2D), as observed in human neonates.[43] Within superficial WM structures, the increase in FA in frontal WM (18.4%) was larger than that in parietal regions (Figure 2D). This has also been identified in human neonatal and pediatric DTI.[44] The internal capsule (IC) had the highest FA value at 3 weeks among distinguished porcine WM structures (Figure 2D). In particular, the highest ranges of FA values were observed in the posterior limb of the IC (PLIC) and the retrolenticular part of the IC compared with other structures (Table 4). In the human WM at 40 postconceptional weeks, FA values of the PLIC were the highest compared with other regions.[45] Consistent with our previous findings using an immunohistological approach,[22] our imaging studies indicate that porcine WM development displays a structure-specific maturation pattern similar to that of human WM.

A lack of cellular investigations in postnatal human brain due to technical and ethical difficulties has prevented the definition of epochs of human WM development that correspond to the porcine model.[22] Oishi et al performed normalization-based brain analysis with detailed anatomic information derived from DTI in human neonates, which demonstrated age-dependent and structure-specific FA changes with different slopes and intercepts.[45] In their study, the FA slope was the highest in the PLIC.[45] The FA of the PLIC in this animal model displays 0.458 ± 0.040 and 0.517 ± 0.024 at 3 and 7 weeks of age, respectively (Table 4). Using regression analysis ($FA=0.0063\times age+0.162$), we identified that FA value in the same porcine WM structure at postnatal 3 and 7 weeks was equivalent to those of human postconceptional 41 to 53 and 53 to 60 weeks, respectively, indicating that developmental time windows in this model correspond with early infancy in human WM. Studies of postmortem human tissue are limited, particularly for analysis of perinatal brain development under normal physiological conditions. Although nonhuman primates share key structural

Table 7. Apparent Diffusion Coefficient in Each WM Region on Postoperative Day 3 and Week 4

CPB Groups	Control		Mild CPB		Severe CPB			
WM Regions	Mean	SD	Mean	SD	Mean	SD	F Test	*P* Value
Day 3*	n=3		n=4		n=6			
GCC	0.944	0.161	0.955	0.048	0.932	0.049	0.092	0.913
BCC	1.059	0.067	0.948	0.116	0.968	0.081	1.434	0.284
SCC	1.044	0.123	0.995	0.071	0.993	0.098	0.301	0.746
ALIC	0.653	0.024	0.661	0.040	0.663	0.037	0.087	0.917
PLIC	0.645	0.029	0.638	0.027	0.641	0.063	0.019	0.981
RLIC	0.730	0.074	0.676	0.006	0.713	0.051	1.190	0.344
M-PVWM	0.734	0.023	0.677	0.042	0.664	0.059	2.178	0.164
L-PVWM	0.680	0.013	0.664	0.084	0.629	0.055	0.822	0.467
PTR	0.774	0.029	0.753	0.035	0.788	0.039	1.178	0.347
SLF	0.765	0.031	0.739	0.036	0.718	0.069	0.736	0.504
CingWM	0.748	0.021	0.706	0.036	0.681	0.047	2.860	0.104
SFWM	0.770	0.074	0.727	0.035	0.702	0.061	1.378	0.296
MFWM	0.766	0.022	0.698	0.034	0.683	0.072	2.313	0.149
IFWM	0.758	0.028	0.739	0.032	0.735	0.068	0.199	0.823
PrCWM	0.709	0.020	0.698	0.035	0.680	0.071	0.321	0.733
SPWM	0.759	0.025	0.734	0.059	0.716	0.057	0.682	0.528
Week 4†	n=3		n=3		n=3			
GCC	0.853	0.126	0.856	0.130	0.908	0.113	0.191	0.831
BCC	0.965	0.104	0.819	0.187	0.875	0.064	0.980	0.428
SCC	0.907	0.093	0.904	0.153	0.923	0.018	0.029	0.972
ALIC	0.670	0.040	0.638	0.070	0.666	0.028	0.379	0.700
PLIC	0.652	0.045	0.587	0.099	0.644	0.046	0.803	0.491
RLIC	0.708	0.055	0.668	0.042	0.704	0.020	0.817	0.486
M-PVWM	0.717	0.050	0.635	0.119	0.700	0.073	0.770	0.504
L-PVWM	0.712	0.047	0.580	0.105	0.661	0.049	2.552	0.158
PTR	0.774	0.035	0.705	0.061	0.791	0.093	1.387	0.320
SLF	0.797	0.047	0.680	0.133	0.779	0.114	1.093	0.394
CingWM	0.772	0.086	0.652	0.147	0.724	0.074	0.961	0.435
SFWM	0.741	0.053	0.670	0.099	0.715	0.020	0.879	0.463
MFWM	0.725	0.046	0.749	0.128	0.711	0.064	0.148	0.866
IFWM	0.800	0.042	0.654	0.148	0.772	0.074	1.836	0.239
PrCWM	0.725	0.040	0.654	0.104	0.698	0.050	0.768	0.505
SPWM	0.743	0.062	0.650	0.096	0.723	0.047	1.426	0.311

ALIC indicates anterior limb of the internal capsule; BCC, body of the corpus callosum; CingWM, cingulum white matter; CPB, cardiopulmonary bypass; GCC, genu of the corpus callosum; IFWM, inferior frontal white matter; L-PVWM, lateral periventricular white matter; MFWM, middle frontal white matter; M-PVWM, medial periventricular white matter; PLIC, posterior limb of the internal capsule; PrCWM, pre-central white matter; PTR, posterior thalamic radiation; RLIC, retrolenticular limb of the internal capsule; SCC, splenium of the corpus callosum; SFWM, superior frontal white matter; SLF, superior longitudinal fasciculus; SPWM, superior-parietal white matter; WM, white matter.

*ADC values are significantly different among 16 WM regions ($F=45.3$, $P<0.0001$) and between CPB groups ($F=7.18$, $P<0.01$) by 2-way ANOVA.

†ADC values are significantly different among 16 WM regions ($F=8.314$, $P<0.001$) and between CPB groups ($F=9.031$, $P<0.001$) by 2-way ANOVA.

characteristics of the human gyrencephalic WM, technical and ethical barriers often prevent direct investigations in these species, especially during early infancy. Thus, our results demonstrate that the postnatal porcine brain is a powerful tool to study normal development and its pathology in the human neonate and infant WM.

Table 8. Percentage Change of Fractional Anisotropy in Each WM Region From Preoperative Period

CPB Group	Control (n=3)		Mild CPB (n=3)		Severe CPB (n=3)		F Test	*P* Value	Control vs Mild CPB	Control vs Severe CPB	Mild CPB vs Severe CPB
WM Region	Mean	SD	Mean	SD	Mean	SD					
GCC	24.034	27.780	38.258	8.435	−26.678	6.516	11.844	0.008	0.350	0.011	0.004
BCC	17.422	2.907	16.811	9.791	−7.725	7.822	11.191	0.009	0.923	0.006	0.007
SCC	8.170	19.079	22.157	15.463	−2.365	11.766	1.837	0.239			
ALIC	15.576	9.076	22.512	7.202	17.429	5.246	0.718	0.526			
PLIC	7.580	4.993	21.934	0.651	9.564	5.418	9.953	0.012	0.006	0.590	0.012
RLIC	−0.780	9.249	13.370	0.568	5.517	11.651	2.041	0.211			
M-PVWM	17.383	2.770	3.271	8.517	9.660	22.834	0.747	0.513			
L-PVWM	5.237	2.074	25.127	6.302	10.902	3.291	17.233	0.003	0.001	0.156	0.007
PTR	5.775	2.087	18.799	5.769	7.095	13.361	2.140	0.199			
SLF	4.788	8.036	7.429	5.698	3.733	12.717	0.126	0.884			
CingWM	7.383	3.855	1.262	13.463	11.048	11.987	0.647	0.556			
SFWM	9.653	5.472	28.158	1.814	5.710	2.769	31.610	0.001	0.001	0.239	<0.001
MFWM	21.757	7.353	21.203	6.317	−2.154	8.057	10.550	0.011	0.929	0.007	0.008
IFWM	10.648	1.709	−5.872	2.556	9.963	26.165	1.133	0.383			
PrCWM	8.168	10.154	10.834	3.909	7.098	5.727	0.220	0.808			
SPWM	4.875	4.381	30.741	0.046	22.685	8.392	17.594	0.003	0.001	0.007	0.121

FA values are significantly different among 16 WM regions ($F=77.9$, $P<0.001$) and between CPB groups ($F=2.5$, $P<0.001$) by 2-way ANOVA. There are significant interactions between WM regions and CPB ($F=8.3$, $P<0.001$). ALIC indicates anterior limb of the internal capsule; BCC, body of the corpus callosum; CingWM, cingulum white matter; CPB, cardiopulmonary bypass; FA, fractional anisotropy; GCC, genu of the corpus callosum; IFWM, inferior frontal white matter; L-PVWM, lateral periventricular white matter; MFWM, middle frontal white matter; M-PVWM, medial periventricular white matter; PLIC, posterior limb of the internal capsule; PrCWM, precentral white matter; PTR, posterior thalamic radiation; RLIC, retrolenticular limb of the internal capsule; SCC, splenium of the corpus callosum; SFWM, superior frontal white matter; SLF, superior longitudinal fasciculus; SPWM, superior parietal white matter; WM, white matter.

Developmental Stage-Dependent WM Vulnerability Against Insults Associated With Congenital Heart Surgery

Using the model, we next assessed FA changes on postoperative day 3 and week 4 following CPB (Figure 1A). FA values on post-CPB day 3 were significantly different among tested WM structures but not among 3 CPB groups (Table 5). On the other hand, at 4 weeks after surgery both WM structures and CPB groups had significant differences in FA values (Table 5). We also found significant interaction between WM regions and CPB groups on postoperative week 4 (Table 5). The interactions among 6 WM subregions and CPB groups in FA value at 4 weeks after surgery are given in Figure 3A. The decrease in FA after CPB was significantly identified in the CC, followed by the frontal superior WM (Figure 3A, Table 6). These regions displayed the largest FA change from postnatal 3 to 7 weeks in normal porcine WM development (Figure 2D). In contrast, the IC and distant projection (DP), which had different DTI characteristics in normal physiological condition including high FAs at 3 weeks of age and low changes from 3 to 7 weeks (Figure 2D), demonstrated no changes at 4 weeks after CPB compared with control (Figure 3A). These results confirm developmental stage-dependent WM vulnerability to brain insults, as shown in studies using rodent and large animal models.[47,48]

FA Changes After CPB are Both Region-Specific and Insult-Dependent and WM at Frontal Cortex is Susceptible to CPB-Induced Insults

On postoperative week 4 (7 weeks of age), CPB significantly affected FA in 4 identified WM regions: GCC, BCC, SFWM, and MFWM (Table 5). On the other hand, no changes in apparent diffusion coefficient were displayed among 3 CPB groups at both day 3 and week 4 after surgery (Table 7). The time-course of FA changes in BCC and SFWM on preoperative and postoperative day 3 and week 4 are also shown in Figure 3B and 3C. Severe CPB resulted in significant FA decreases in the corpus callosum (GCC, BCC) and subcortical WM of the frontal cortex (SFWM, MFWM) compared with control (Table 5). Interestingly a significant FA increase was seen in SFWM following mild CPB (Figure 3F). In GCC, BCC, and SFWM, FA was highest after mild CPB and lowest in severe CPB, and there was a significant difference between mild and severe CPB (Table 5). In our study design, mild CPB insult included

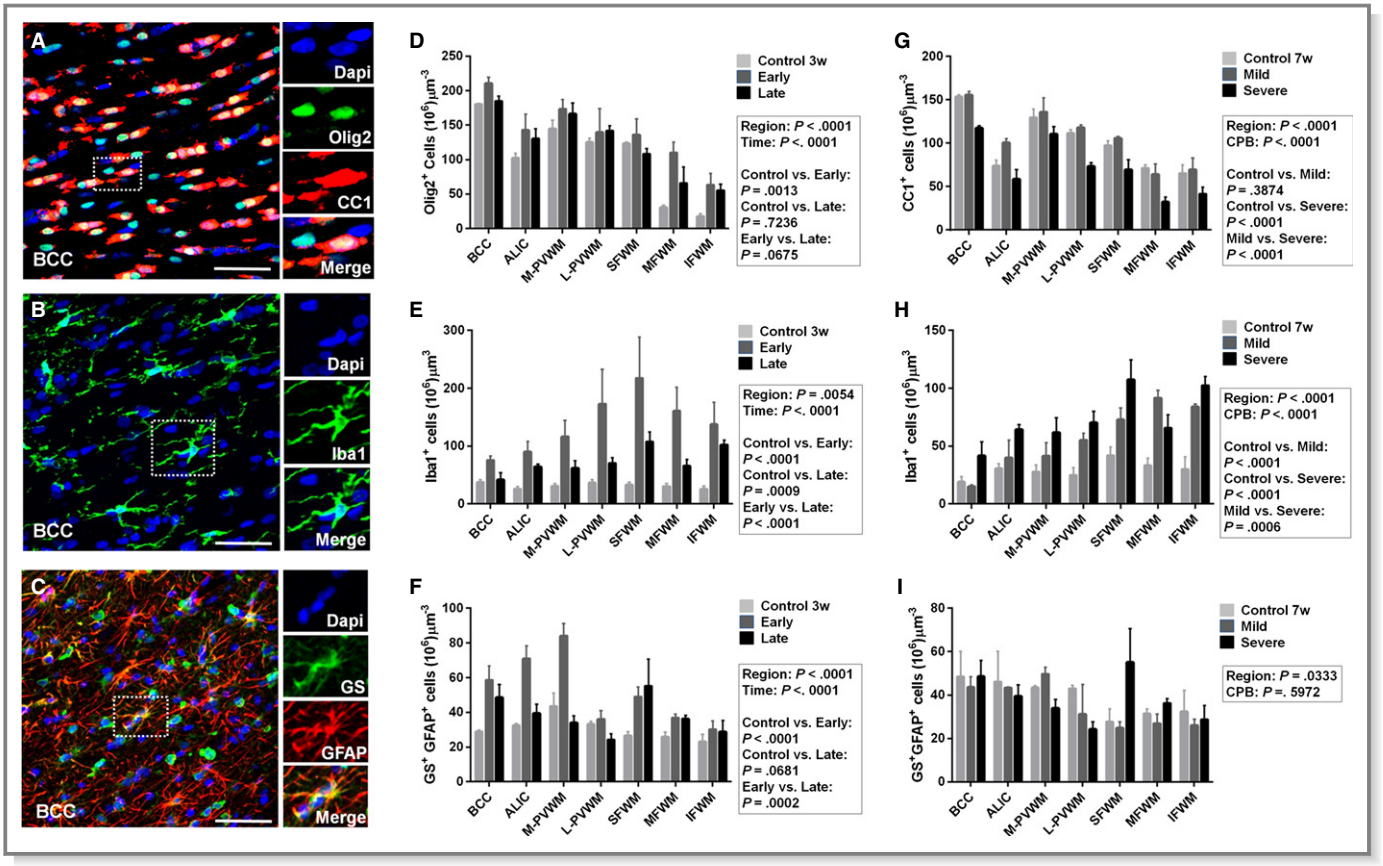

Figure 4. CPB-induced cellular events in the developing WM include an increase in oligodendrocyte lineage cells and their dysmaturation, acute astrogliosis, and prolonged microglial expansion. A, Olig2$^+$ oligodendrocyte lineage cells and CC1$^+$ mature oligodendrocytes. B, Iba1$^+$ microglia. C, GS$^+$GFAP$^+$ astrocytes. D, There is an increase in Olig2$^+$ oligodendrocyte lineage cells early after severe CPB, but not at post-CPB 4 weeks (n=3-5 in each). More data are presented in Table 9. E, Iba1$^+$ microglial expansion is observed both early and late following severe CPB (n=3-5 in each). More data are presented in Table 9. F, Severe CPB results in acute astroligosis (n=3-5 in each). More data are presented in Table 9. These cellular events following severe CPB vary among the 7 WM regions analyzed (D through F). G, There is a reduction of CC1$^+$ mature oligodendrocytes after severe CPB, but not after mild CPB, 4 weeks postoperatively (n=3 in each). More data are presented in Table 10. H, Both mild and severe CPB insults cause prolonged microglial expansion (n=3 in each). More data are presented in Table 10. I, There are no differences in GS$^+$GFAP$^+$ astrocyte numbers among the 3 CPB groups at postoperative week 4 (n=3 in each). More data are presented in Table 10. Early indicates postoperative days 3 and 10. Late indicates postoperative week 4. Data are shown as mean±SEM. ALIC indicates anterior limb of the internal capsule; BCC, body of the corpus callosum; CPB, cardiopulmonary bypass; IFWM, inferior frontal white matter; L-PVWM, lateral periventricular white matter; MFWM, middle frontal white matter; M-PVWM, medial periventricular white matter; SFWM, superior frontal white matter; w, weeks; WM, white matter.

CPB-induced SIRS, whereas both SIRS and I/R injury were involved in severe CPB (Figure 1A and Table 1). Thus, our data suggest insult-dependent FA alterations in developing WM following cardiac surgery.

We further analyzed percentage changes of FA from preoperation to week 4 postsurgery among 3 groups (Table 8). Within 16 WM areas, severe-CPB significantly decreased FA in GCC, BCC, and MFWM (Table 8). These 3 regions had a large FA increase (17% to 24%) in control animals during the time period analyzed (Table 8). The results confirm the developmental stage-dependent WM vulnerability to CPB-induced insults. There were significant increases in FA after mild CPB in 4 WMs (PLIC, L-PVWM, SFWM, and superior parietal WM) compared with control (Table 8). In superior parietal WM, severe CPB also resulted in FA increase (Table 8), suggesting that FA alteration following CPB varies among WM regions.

Within 6 WM subregions (Table 2), there were no differences in percentage changes in DP (P=0.53), deep WM association (P=0.92), and frontal superficial WM (P=0.32) among the 3 CPB groups. On the other hand, the corpus callosum displayed a significant decrease in FA after severe CPB (Figure 3D). In the IC and parietal superficial WM there were no differences between control and severe CPB, whereas mild CPB caused an FA increase compared with control (Figure 3E and 3F). Altogether our results

Table 9. Comparison of Cell Numbers Between Time Period Groups After Severe CPB Stratified by WM Region

Time Periods	Control (n=5)		Early (n=3)		Late (n=3)		Control vs Acute	Control vs Long Term	Acute vs Long Term
WM Regions	Mean	SD	Mean	SD	Mean	SD			
$Olig2^+$ oligodendrocytes									
BCC	180.0	3.4	210.5	15.8	184.7	13.1			
ALIC	102.4	15.2	142.8	40.4	130.3	25.0	0.081		
M-PVWM	144.6	27.9	173.1	23.9	166.3	27.3			
L-PVWM	125.1	12.6	139.6	59.5	141.6	12.9			
SFWM	123.1	4.3	136.1	39.2	108.2	13.8			
MFWM	30.4	6.3	110.2	26.5	65.8	41.0	0.001		
IFWM	17.8	6.3	63.2	28.9	55.3	16.0			
$Olig2^+CC1^-$ immature oligodendrocytes									
BCC	66.8	16.0	64.9	17.3	67.2	15.4			
ALIC	23.1	10.9	40.4	18.3	71.8	42.6		0.003	
M-PVWM	39.6	18.0	42.8	17.9	55.6	17.4			
L-PVWM	28.0	23.4	36.4	34.2	68.1	11.4		0.015	
SFWM	22.2	10.9	16.1	6.8	38.8	7.4			
MFWM	6.9	2.3	23.2	13.1	33.6	31.5			
IFWM	3.4	1.6	33.9	19.3	13.7	5.3			
$Olig2^+CC1^+$ mature oligodendrocytes									
BCC	113.2	14.6	145.6	13.8	117.5	4.3	0.030		
ALIC	79.2	5.1	102.3	26.5	58.5	19.1			0.007
M-PVWM	105.0	26.8	130.4	15.7	110.6	14.2			
L-PVWM	97.1	11.5	103.2	28.1	73.4	7.3			
SFWM	101.0	10.9	120.1	35.2	69.4	20.4		0.037	0.001
MFWM	23.5	4.0	87.0	14.7	32.2	9.7	<0.001		0.001
IFWM	15.5	4.0	40.6	5.7	41.5	13.4			
$Iba1^+$ microglia									
BCC	37.4	9.8	75.6	12.7	41.7	21.0			
ALIC	25.8	10.5	89.9	32.2	64.3	6.9			
M-PVWM	30.5	10.1	116.3	49.2	61.7	21.8	0.013		
L-PVWM	36.5	11.7	172.9	103.8	70.3	16.9	<0.001		0.007
SFWM	32.9	10.1	217.3	123.8	107.4	29.6	<0.001	0.037	0.004
MFWM	30.5	10.5	160.7	71.6	65.6	19.5	<0.001		0.014
IFWM	25.5	11.9	137.5	66.2	102.3	13.4	0.001	0.030	
GS^+GFAP^+ astrocytes									
BCC	28.9	1.6	58.6	14.2	48.6	12.7	0.003		
ALIC	32.4	1.9	71.0	12.9	39.5	8.9	<0.001		0.002
M-PVWM	43.5	13.0	84.1	12.3	34.0	6.9	<0.001		<0.001
L-PVWM	33.2	2.7	36.1	8.3	24.2	6.1			
SFWM	26.6	3.9	49.0	9.7	55.1	27.0	0.034	0.005	
MFWM	25.9	4.7	36.9	3.9	36.2	3.7			
IFWM	23.0	7.5	30.2	8.5	28.8	11.4			

ALIC indicates anterior limb of the internal capsule; BCC, body of the corpus callosum; CPB, cardiopulmonary bypass; IFWM, inferior frontal white matter; L-PVWM, lateral periventricular white matter; MFWM, middle frontal white matter; M-PVWM, medial periventricular white matter; SFWM, superior frontal white matter; WM, white matter.

Table 10. Comparison of Cell Numbers Between CPB Groups Stratified by WM Region

CPB Group	Control (n=3)		Mild CPB (n=3)		Severe CPB (n=3)		Control vs Mild CPB	Control vs Severe CPB	Mild CPB vs Severe CPB
WM Region	Mean	SD	Mean	SD	Mean	SD			
$Olig2^+$ oligodendrocytes									
BCC	181.0	7.9	190.2	4.7	184.7	13.1			
ALIC	161.6	34.3	173.5	38.1	166.3	27.3			
M-PVWM	184.7	13.1	139.3	18.2	100.1	34.5	0.044	<0.001	
L-PVWM	139.3	18.2	137.3	4.3	141.6	12.9			
SFWM	118.8	3.6	126.4	5.9	108.2	13.8			
MFWM	100.3	14.7	100.1	34.5	65.8	41.0			
IFWM	105.8	18.5	134.4	15.7	55.3	16.0		0.021	<0.001
$Olig2^+CC1^-$ immature oligodendrocytes									
BCC	30.6	14.7	31.9	4.1	67.2	15.4			
ALIC	13.4	10.7	16.1	1.5	71.8	42.6		0.003	0.004
M-PVWM	32.3	27.7	37.5	23.8	55.6	17.4			
L-PVWM	27.9	17.3	19.4	2.5	68.1	11.4		0.051	0.013
SFWM	21.5	7.5	20.7	9.4	38.8	7.4			
MFWM	29.2	19.7	36.2	14.4	33.6	31.5			
IFWM	40.5	22.1	64.9	38.9	13.7	5.3			0.009
$Olig2^+CC1^+$ mature oligodendrocytes									
BCC	153.3	4.1	155.4	6.9	117.5	4.3		0.010	0.006
ALIC	73.9	11.6	100.5	8.4	58.5	19.1			0.002
M-PVWM	129.4	17.5	136.0	27.7	110.6	14.2			
L-PVWM	111.4	6.9	117.9	5.4	73.4	7.3		0.006	0.001
SFWM	97.3	9.5	105.7	3.6	69.4	20.4			0.009
MFWM	71.1	7.2	63.9	21.2	32.3	9.7		0.005	0.027
IFWM	65.2	17.3	69.5	23.1	41.5	13.4			
$Iba1^+$ microglia									
BCC	19.0	7.8	15.1	2.5	41.7	21.0			
ALIC	30.6	7.1	39.8	26.5	64.3	6.9		0.039	
M-PVWM	27.8	10.1	41.4	20.2	61.7	21.9		0.037	
L-PVWM	24.8	11.4	55.2	10.2	70.3	16.9		0.003	
SFWM	41.8	12.7	73.0	17.1	107.4	29.6		<0.001	0.034
MFWM	33.2	11.3	91.6	11.3	65.7	19.5	<0.001	0.049	
IFWM	29.9	18.7	84.0	3.6	102.3	13.4	<0.001	<0.001	
GS^+GFAP^+ astrocytes									
BCC	48.5	20.3	43.6	8.4	48.6	12.7			
ALIC	46.2	24.1	43.4	0.7	39.5	8.9			
M-PVWM	43.4	1.5	49.7	5.5	34.0	6.9			
L-PVWM	43.0	2.7	31.2	23.6	24.2	6.1			
SFWM	27.6	10.4	24.9	4.7	55.1	27.0		0.033	0.017
MFWM	31.4	3.9	27.0	7.5	36.3	3.7			
IFWM	32.4	16.9	26.0	4.9	28.8	11.4			

ALIC indicates anterior limb of the internal capsule; BCC, body of the corpus callosum; CPB, cardiopulmonary bypass; IFWM, inferior frontal white matter; L-PVWM, lateral periventricular white matter; MFWM, middle frontal white matter; M-PVWM, medial periventricular white matter; SFWM, superior frontal white matter; WM, white matter.

Table 11. Fractional Anisotropy and Cellular Changes

Variable	r_s	*P* Value	Equation
Control			
$Olig2^+$ oligodendrocytes	0.079	0.735	
$Olig2^+CC1^-$ immature oligodendrocytes	−0.261	0.254	
$Olig2^+CC1^+$ mature oligodendrocytes	0.183	0.428	
$Iba1^+$ microglia cells	−0.414	0.062	
GS^+GFAP^+ astrocytes	0.369	0.099	
Post-CPB acute			
$Olig2^+$ oligodendrocytes	0.389	0.041	Y=292.0X+19.01
$Olig2^+CC1^-$ immature oligodendrocytes	0.345	0.084	
$Olig2^+CC1^+$ mature oligodendrocytes	0.356	0.066	
$Iba1^+$ microglia cells	0.001	0.998	
GS^+GFAP^+ astrocytes	0.389	0.045	Y=103.1X+9.695
Post-CPB week 4			
$Olig2^+$ oligodendrocytes	0.364	0.018	Y=199.0X+52.12
$Olig2^+CC1^-$ immature oligodendrocytes	0.047	0.767	
$Olig2^+CC1^+$ mature oligodendrocytes	0.401	0.009	Y=182.0X+17.52
$Iba1^+$ microglia cells	−0.506	0.001	Y=−161.8X+129.2
GS^+GFAP^+ astrocytes	0.047	0.767	

CPB indicates cardiopulmonary bypass.
In equations Y is cells per microm ^3 and X is FA.

demonstrated both region-specific and insult-dependent FA changes after cardiac surgery.

CPB-Induced Cellular Events in the Developing WM Include an Increase in Oligodendrocyte Lineage Cells and Their Dysmaturation, Acute Astrogliosis, and Prolonged Microglial Expansion

To understand cellular events associated with changes in WM anisotropy, we analyzed changes of major cellular components including $Olig2^+$ oligodendrocyte lineage cells, $Olig2^+CC1^-$ immature oligodendrocytes, $Olig2^+CC1^+$ mature oligodendrocytes, $Iba1^+$ microglia, and GS^+GAFP^+ astrocytes (Figure 4A through 4C). Consistent with our previous findings, we observed (1) an increase in oligodendrocyte lineage cells; (2) microglial expansion; and (3) astrogliosis early after severe CPB (Figure 4D through 4F, Table 9).[22,23,49] At post-CPB week 4 we also observed severe CPB-induced oligodendrocyte dysmaturation (ie, reduction of $CC1^+$ mature oligodendrocytes paired with an increase in $Olig2^+CC1^-$ immature oligodendrocytes) and prolonged microglial expansion following both mild and severe CPB (Figure 4G and 4H, Table 10).[22,23] On the other hand, astrocyte numbers were consistent in both groups on post-CPB week 4 (Figure 4I). These cellular events caused by CPB significantly varied among the 7 WM regions analyzed (Figure 4D through 4I).

FA Increases Parallel Cellular Processes of WM Maturation During Normal Development

In order to determine cellular events associated with changes in WM anisotropy, we first compared the change of cell numbers in 7 regions with FA of each corresponding region in control WM. There were no relationships between FA and cellular changes in a linear regression model (Table 11); on the other hand, we observed an inverted U-shape pattern between FA and oligodendrocyte cell numbers (Figure 5A). When WM subdivisions—(1) CC; (2) IC; (3) DP; (4) SFWM (Table 2)—were categorized and ranked based on mean FA value, numbers of oligodendrocyte and mature oligodendrocyte cells at CC (FA=0.41) and DP (FA=0.45) significantly increased compared with SFWM where lower FA (0.37) was measured (Figure 4B and 4C). Conversely, the numbers in IC (FA=0.51) significantly decreased compared with CC and DP (Figure 5B and 5C). Cellular processes underlying WM maturation involve expansion of oligodendrocyte lineages and axonal myelination through mature oligodendrocytes,

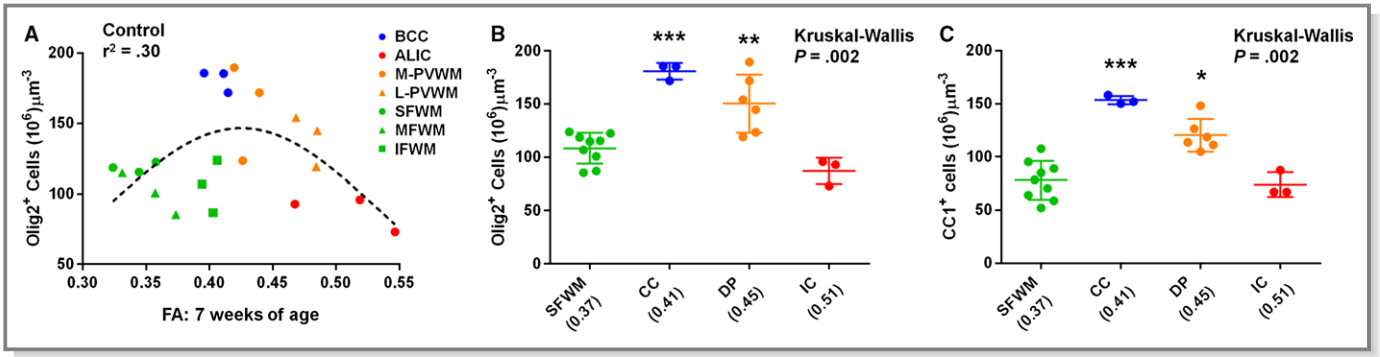

Figure 5. FA increases parallel cellular processes of WM maturation during normal development. A, Plot of FA and Olig2$^+$ oligodendrocyte cell number in 7 WM regions shows an inverted U-shape pattern among controls at 7 weeks of age (n=3 animals). B and C, When 4 WM subregions are ranked based on mean FA from left to right on X-axis, changes of Olig2$^+$ oligodendrocyte (B) and CC1$^+$ mature oligodendrocyte cell (C) numbers display cellular processes underlying WM maturation that involve expansion of oligodendrocyte lineages and myelination through mature oligodendrocytes, followed by a decline of mature oligodendrocytes while maintaining myelination (n=3 animals). *P=0.05 vs SFWM, **P<0.05 vs IC, ***P<0.05 vs SFWM and IC by the Kruskal-Wallis followed by Mann-Whitney U-tests. ALIC indicates anterior limb of the internal capsule; BCC, body of the corpus callosum; CPB, cardiopulmonary bypass; FA, fractional anisotropy; IC, internal capsule; IFWM, inferior frontal white matter; L-PVWM, lateral periventricular white matter; MFWM, middle frontal white matter; M-PVWM, medial periventricular white matter; SFWM, superior frontal white matter; WM, white matter.

followed by a decline of mature oligodendrocytes with maintaining myelination.[37,40,41] Therefore, our results confirm FA as a useful image biomarker for WM maturation under normal physiological conditions in this model. Linear and nonlinear relations of FA with microglia and astrocyte cell numbers were not observed in control animals (Table 11).

Normal Correlation of FA With Oligodendrocyte Lineages Are Altered After Cardiac Surgery and CPB-Induced Astrogliosis and Microglial Expansion

Next we analyzed the correlation between FA and cellular events in both mild and severe CPB groups. When cellular changes were divided between the acute period and week 4 following CPB, inverted U-shaped distributions between FA and oligodendrocyte and mature oligodendrocyte numbers (Figure 5A through 5C), which we observed in control WM, were disrupted in both time periods following CPB, although linear relations of FA with oligodendrocytes and mature oligodendrocytes were seen (Figure 6A and 6C). The results demonstrate that CPB-induced cellular events in oligodendrocyte lineages—acute expansion and dysmaturation—alter the sequence of FA with oligodendrocyte maturation in normal WM development.

In control animals, FAs were not associated with astrocyte and microglia numbers (Table 11). However, following CPB, FA changes were positively associated with GS$^+$GFAP$^+$ astrocyte numbers in the acute postoperative period (Figure 6B). Interestingly, a negative correlation between FA and microglia number was displayed at week 4 after CPB (Figure 6D). Together our results demonstrate that both CPB-induced astrogliosis and microglial expansion affect FA changes after cardiac surgery.

FA at 4 Weeks After Cardiac Surgery Enables Identification of CPB-Induced Cellular Events in Developing WM

The aforementioned results suggest complex correlations between FA and cellular changes after cardiac surgery. In other animal models the relationship between DTI indices and neuropathology also became less straightforward in complex pathological conditions.[15] For instance in a mouse model of myelination injury, histology showed severe demyelination and inflammation, whereas diffusivity measured by in vivo DTI showed no significant difference from control animals.[50,51] In order to test such a scenario, we categorized 7 WMs into regions with FA change (BCC, SFWM, MFWM) and without FA change (anterior limb of the internal capsule, M-PVWM, L-PVWM, IFWM, Table 6) and compared the correlation of FA with the histological data. We found a positive relation of FA with oligodendrocyte and mature oligodendrocyte numbers on post-CPB week 4: conversely, FA was negatively correlated with microglia number (Figure 6C and 6D, Table 11). When the correlation was compared between WMs with and without FA changes, slopes significantly differed between 2 categorized regions (Figure 7A and 7B). In each correlation, we found better fitness in the area with FA change compared with the WM without the change (Figure 7A and 7B), demonstrating that FA changes after CPB correspond with pathological events such as the reduction of mature oligodendrocytes and increase in microglia. Indeed, in BCC, SFWM, and MFWM, where significant FA reductions were seen after severe CPB

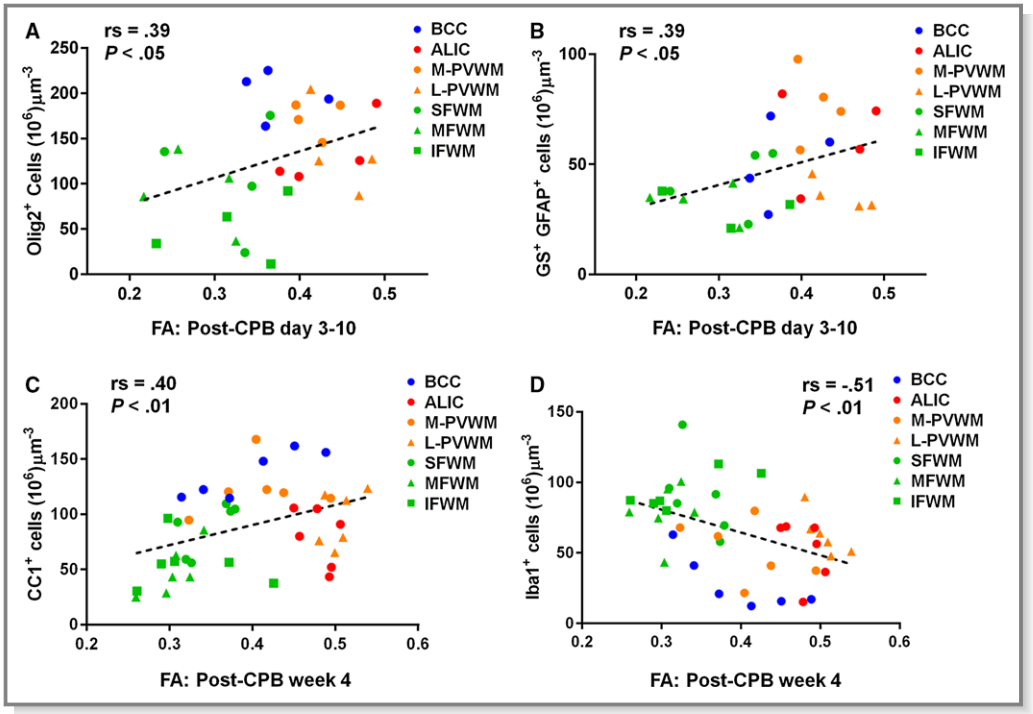

Figure 6. The association between FA and cellular processes of WM maturation is altered after cardiac surgery. CPB-induced oligodendrocyte dysmaturation, astrogliosis, and microglial expansion affect FA changes, and FA on postoperative week 4 demonstrates CPB-induced cellular alterations including reduction of mature oligodendrocytes and microglial expansion. A and B, FA changes are positively associated with Olig2$^+$ oligodendrocyte numbers (A) and GS$^+$GFAP$^+$ astrocyte numbers (B) in the acute period following CPB by Spearman rank-order correlation coefficient (n=4 animals). C, Positive linear relations of FA with CC1$^+$ mature oligodendrocytes are seen at week 4 after CPB by the Spearman rank-order correlation coefficient rather than inverted U-shape distributions (n=6 animals). D, There is a moderate negative association between FA and microglia number 4 weeks postoperatively by the Spearman rank-order correlation coefficient (n=6 animals). More data are presented in Table 11. ALIC indicates anterior limb of the internal capsule; BCC, body of the corpus callosum; CPB, cardiopulmonary bypass; FA, fractional anisotropy; IFWM, inferior frontal white matter; L-PVWM, lateral periventricular white matter; MFWM, middle frontal white matter; M-PVWM, medial periventricular white matter; SFWM, superior frontal white matter; WM, white matter.

(Figure 3B and 3C, Table 5), a lower number of mature oligodendrocytes paired with a higher microglia number was displayed (Figure 4G and 4H, Table 10). There were significant increases in FA following mild CPB compared with severe CPB in BCC and SFWM (Figure 3B and 3C). In these regions oligodendrocyte numbers in mild CPB were higher than those with severe CPB, although microglia numbers were lower (Table 10). Together our results suggest that FA changes on postoperative week 4 enable identification of CPB-induced cellular alterations including reduction of mature oligodendrocytes and microglial expansion.

On the other hand, we did not observe such differences between mild and severe CPB insults in corrections of FA with oligodendrocytes, mature oligodendrocytes, and microglia (Figure 7C and 7D). Although both FA and cellular alterations significantly vary according CPB-induced insults (Table 10, Figure 4), our analyses indicate that the relations between FA changes and cellular events are not affected by distinct pathological conditions due to CPB. Altogether our results demonstrate that FA is a powerful biomarker to define WM cellular alterations after cardiac surgery.

Effects of Mature Oligodendrocyte and Microglia Numbers on FA Reduction Following CPB

Neurocognitive deficits in adolescents with D-transposition of the great arteries repaired in infancy are associated with WM FA reduction.[17] Changes in FA during the early postnatal period persist into adolescence and young adulthood in subjects born prematurely.[8] Thus, preventing or recovering WM FA reduction after neonatal cardiac surgery could be a promising avenue to improve neurological impairment in CHD patients. In order to develop a cellular-based treatment strategy, we investigated the

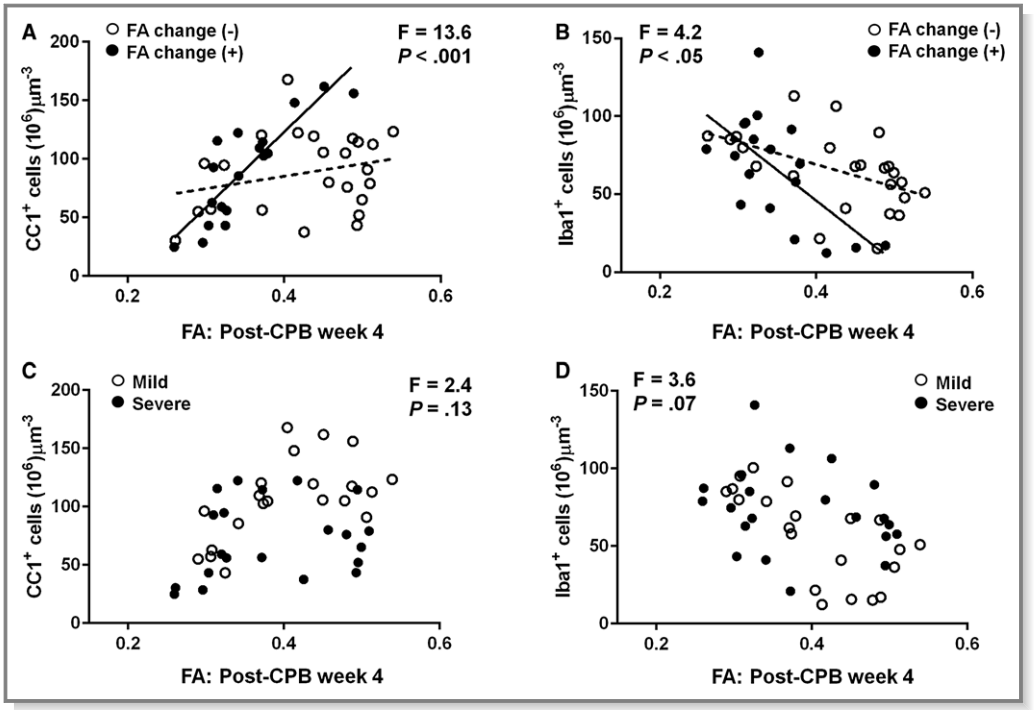

Figure 7. FA is a powerful biomarker to define WM cellular alterations after cardiac surgery. A and B, When the correlation is compared in WM areas between with and without FA changes (BCC, SFWM, MFWM vs ALIC, M-PVWM, L-PVWM, IFWM), better fits in positive FA relation with mature oligodendrocytes (A) and negative association with microglia (B) are observed in the area with FA change (black line) compared with the WM without change (dotted line), suggesting that FA changes on postoperative week 4 enable identification of CPB-induced cellular alterations (n=6 animals). C and D, There is an unchanged relation between FA and the number of mature oligodendrocyte cells (C) and microglia (D) between mild and severe CPB groups (n=6 animals). ALIC indicates anterior limb of the internal capsule; BCC, body of the corpus callosum; CPB, cardiopulmonary bypass; FA, fractional anisotropy; IFWM, inferior frontal white matter; L-PVWM, lateral periventricular white matter; MFWM, middle frontal white matter; M-PVWM, medial periventricular white matter; SFWM, superior frontal white matter; WM, white matter.

effects of mature oligodendrocyte and microglia cell numbers on FA reduction after CPB.

For the analyses we first examined 2 cutoff values, (1) 1 SD below the mean FA and (2) 2 SDs below the mean FA, in order to compare the definition with better fit for the estimation of cellular events associated with CPB-induced FA reduction. Our analyses identified that the stronger relationship was between FA reduction >1 SD and change in mature oligodendrocytes relative to control. The area under the ROC curve was 0.800, which represents excellent predictive accuracy (95% confidence interval 0.652-0.951, $P<0.001$) between CPB-induced FA reduction and the change in number of mature oligodendrocytes relative to control (Table 12). The box-and-whisker plot shows that the change in number was considerably larger when FA reduction was >1 SD. The change was in the negative direction when FA decreased after CPB (Figure 8A). The Youden J-index revealed that the optimal cutoff value for predicting FA reduction >1 SD was a decrease of 8 or more in the density of WM mature oligodendrocytes, which translated into a sensitivity of 91% and a specificity of 76%. From logistic regression, a change in number of at least −8 compared to control was associated with an odds of FA reduction >1 SD of over 30 (odds ratio=30.4, 95% confidence interval 5.2-178.4, $P<0.001$). The probability curve illustrates negative effects of mature oligodendrocyte numbers on FA reduction (Figure 8B). For example, decreases of 20 and 40 mature oligodendrocytes (per 100 μm^3) are associated with a probability of FA reduction of 60% and 80%, respectively (Figure 8B, Table 13).

Although the relation was less strong compared with the mature oligodendrocyte number, FA reductions were also associated with an increase in microglia cells relative to control (Figure 8C). The area under the receiver operating characteristic curve in the number of microglia demonstrated predictive accuracy of a significant FA reduction (Table 12), such that the increase in 80 WM microglia cells (per 100 μm^3) was associated with a nearly 80% probability in FA reduction following CPB (Figure 8D, Table 14). Interestingly, our theoretical curves showed that no changes of mature oligodendrocyte and microglia numbers relative to control are still associated with 37% and 25% chances in FA

Table 12. Likelihood Ratio Test as Fractional Anisotropy Reduction Relates to Changes in Mature Oligodendrocyte and Microglia Cells

	LRT	*P* Value	AUC	95%CI
All 7 WM regions (n=42)				
Change in mature oligodendrocytes	10.03	0.002	0.800	0.652 to 0.951
Change in microglia cells	4.43	0.035	0.720	0.558 to 0.884
BCC, SFWM, MFWM (n=18)				
Change in mature oligodendrocytes	24.73	<0.0001	1.000	0.998 to 1.000
Change in microglia cells	0.71	0.405	0.650	0.374 to 0.926

AUC indicates area under a quantity-time curve; BCC, body of the corpus callosum; CI, confidence interval; FA, fractional anisotropy; LRT, likelihood ratio test from logistic regression; MFWM, middle frontal white matter; SFWM, superior frontal white matter; WM, white matter.

reduction in each WM region (Figure 8B and 8D). The results suggest the notion that other cellular events secondary to CPB also contributed to FA reduction after cardiac surgery.

Discussion

This study is the first to reveal region-specific FA changes in the porcine WM similar to those that occur in humans and to define corresponding time periods in human WM development. In addition, we identify developmental stage-dependent WM vulnerability against insults associated with cardiac surgery and reveal that WM regions in the frontal cortex are particularly susceptible. Moreover, our data demonstrate region-specific and insult-dependent FA alterations using an animal model anatomically and physiologically similar to humans. In conjunction with detailed cellular assays, the present study also determines that alterations of WM microstructure are affected by CPB-induced oligodendrocyte dysmaturation, astrogliosis, and microglial expansion. Furthermore, FA enables capturing such cellular events postoperatively. Finally, our study also defines a targeted cellular window for reducing the risk of FA reduction, thus contributing to developing a cellular-based treatment strategy for the improvement of neurodevelopmental impairment in the CHD population.

The tremendous power of transgenic/gene-knockout technologies in rodent animal models has led to great success in developing our understanding of cellular/molecular processes underlying brain development and its pathology. However, there is a growing need for a large-animal model for better transition of discoveries derived from rodent studies to clinically relevant questions. Our previous attempt to define the epochs in human WM development that correspond to this porcine model was prevented by a lack of cellular investigations in the postnatal human brain.[22] However, the clinically relevant DTI approach in this study has been able to identify corresponding time windows of porcine WM relative to human WM development. Our results demonstrate that FA at postnatal 3 and 7 weeks in our model is equivalent to those of the early infant stage in the human (postconception 41-53 and 53-60 weeks), contributing to a better understanding of CPB-induced WM alteration in human infants. A wide variety of brain regions possess distinguished developmental time courses, and the diversity differs among various species. Research through innovative imaging technologies is now producing a revolutionary new dynamic picture of the development and pathology in the human brain.[52] Introducing advanced neurotechnologies into gyrencephalic animals including swine and lambs, as we performed in this study, will provide a wealth of bidirectional information in the research directed toward complex human brain development and a wide range of neurodevelopmental disorders.

Postimage processing of MRI data is advancing rapidly. Nevertheless, defining/comparing DTI indices in all regions of the complex human WM are labor-intensive and time-consuming procedures that prevent rapid feedback as valid biomarkers for clinical brain injury. Within various WM areas the present study found significant FA alterations in the corpus callosum (GCC, BCC) and subcortical WM (SFWM, MFWM) in the frontal cortical lobe after CPB, suggesting that FA in the frontal cortex should be a clinically relevant biomarker in WM injury after cardiac surgery. The frontal cortex plays an essential role in executive function, social cognition, and attention,[53-55] and the connectivity through WM in those regions is crucial for proper development of such neurological functions.[9,56] Because impairments in executive function, social cognition, and/or attention are well documented in patients with CHD,[1,3,57] our data also indicate that reducing and recovering WM alterations of the frontal cortex will likely improve lifelong neurodevelopmental consequences in the CHD population.

Our findings suggest that the regions most resistant to FA reduction maintained their mature oligodendrocyte population and inhibited microglial expansion after CBP. Because of our study design, we were unable to determine primary cellular events underlying CPB-induced FA alteration or to verify relationships between cellular events and FA changes observed in the present study. On the other hand, our assay regarding risk analysis in FA reduction on mature oligodendrocytes shows more statistical power compared with microglia number. When the analyses were restricted to BCC, SFWM, and MFWM, where significant FA reductions were observed at post-CPB week 4, the relationship in FA reduction was highly significant for decreased mature

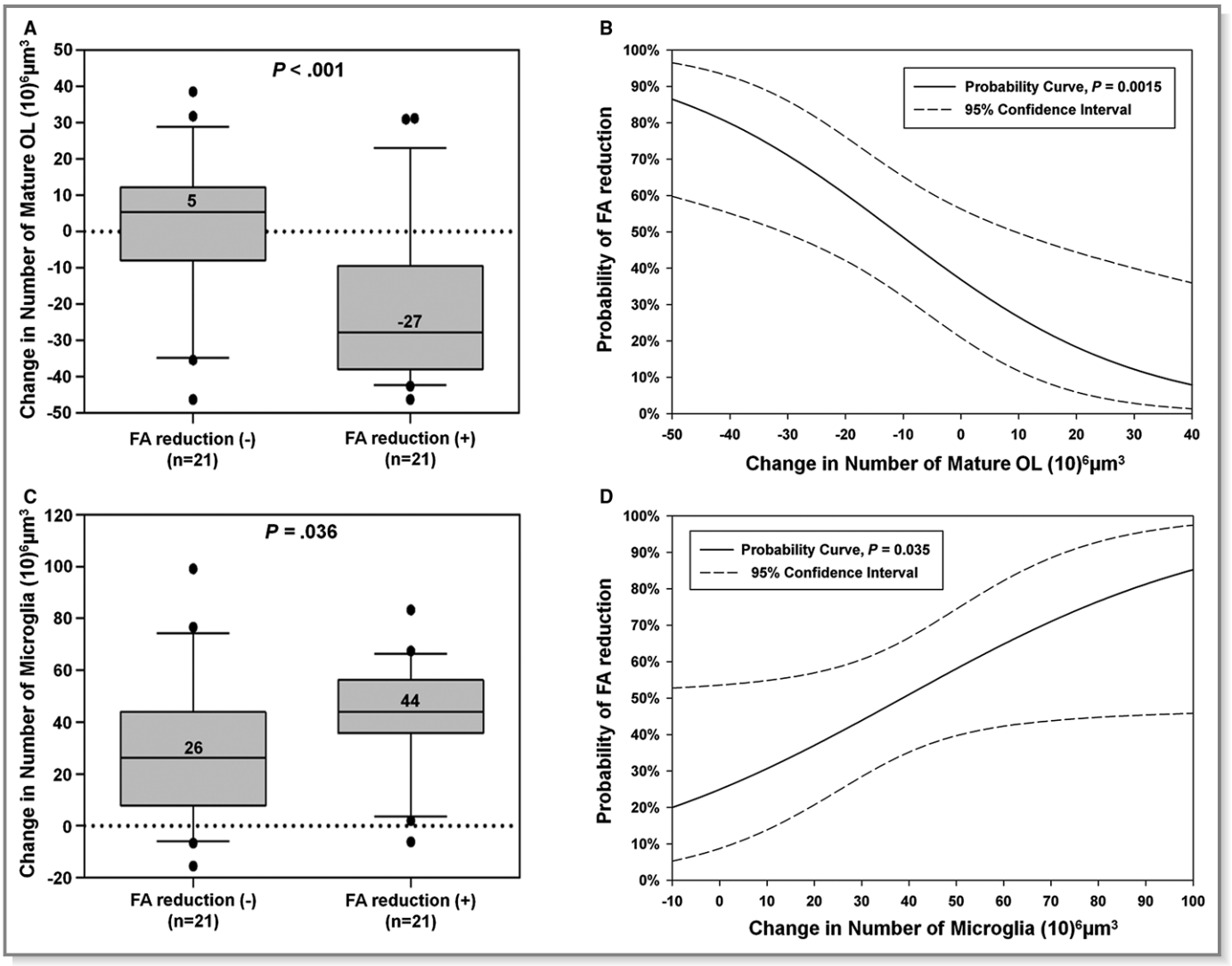

Figure 8. Regions most resilient to CPB-induced FA reduction maintain mature oligodendrocytes and inhibit microglial expansion. A, The box-and-whisker plot for mature oligodendrocyte number relative to control on post-CPB week 4. There are significant reductions in the change of number in FA reduction-positive WM (−21.7±21.5) compared with FA reduction-negative WM (+0.1±20.8) by Mann-Whitney U-test. Median values are presented in the box-and-whisker plot. B, Probability curves of FA reduction as a function of mature oligodendrocyte number relative to control on post-CPB week 4 indicate negative effects of mature oligodendrocyte numbers on FA reduction. C, The box-and-whisker plot for microglia number relative to control. Significant increase in the change of number is observed in FA reduction-positive WM (+42.4±21.4) compared with FA reduction-negative WM (+28.9±28.4) by Mann-Whitney U-test. Median values are presented in the box-and-whisker plot. D, Probability curves of FA reduction as a function of the microglia number relative to control on post-CPB week 4 illustrate positive effects of microglia numbers on FA reduction. CPB indicates cardiopulmonary bypass; FA, fractional anisotropy; OL, oligodendrocyte. More data are presented in Tables 13 and 14.

oligodendrocytes (area under the curve 1.000); however, the change in microglia number was not correlated with FA reduction (Table 12). The results may indicate that restoring mature oligodendrocytes can be primarily targeted to improve microstructural alterations of developing WM. A recent study using a rodent model of developmental WM injury has demonstrated that heparin-binding epidermal growth factor after hypoxic exposure reduced oligodendrocyte death, promoted oligodendrocyte generation, and improved functional/behavioral recovery through endogenous repair mechanisms.[58] Several failures of clinical trials investigating treatment of ischemic brain injury have spurred a consensus that supports the need to determine cross-species efficacy of new therapies. The effects of drugs in pigs resemble the effects in humans more closely than other laboratory animals.[59] Therefore, our unique animal model may lead to a highly translational study to develop new pharmacological treatments for WM injury in children with CHD as well as other neurodevelopmental disorders such as preterm infants.

Table 13. Change in Mature Oligodendrocytes and Probability of Fractional Anisotropy Reduction >1 SD

Change in Number of Mature Oligodendrocytes (per 100 μm^3)	Probability (%)	95% Confidence Interval
−50	86	60% to 97%
−45	83	58% to 95%
−40	80	55% to 93%
−35	76	52% to 90%
−30	71	49% to 86%
−25	66	46% to 81%
−20	60	42% to 76%
−15	55	37% to 71%
−10	49	32% to 65%
−5	43	26% to 60%
0	37	21% to 56%
5	31	16% to 53%
10	27	12% to 50%
15	22	8% to 47%
20	18	6% to 44%
25	15	4% to 42%
30	12	3% to 40%
35	10	2% to 38%
40	8	1% to 35%

Table 14. Change in Microglia and Probability of Fractional Anisotropy Reduction >1 SD

Change in Number of Microglia (per 100 μm^3)	Probability (%)	95% Confidence Interval
−10	20	5% to 52%
−5	22	7% to 53%
0	25	9% to 54%
5	28	11% to 54%
10	31	14% to 55%
15	34	17% to 56%
20	37	21% to 57%
25	40	25% to 59%
30	44	28% to 61%
35	47	32% to 63%
40	51	35% to 67%
45	55	38% to 70%
50	58	40% to 75%
55	62	41% to 79%
60	65	42% to 82%
65	68	43% to 86%
70	71	44% to 89%
75	74	44% to 91%
80	77	45% to 93%
85	79	45% to 95%
90	81	45% to 96%
95	83	46% to 97%
100	85	46% to 98%

Our statistical model suggests that other cellular events also contributed to CPB-induced FA changes. Certainly, myelination and/or axonal swelling would play an important role in alterations of FA after cardiac surgery.[15,60] Electron microscopy is required to analyze/define such structural changes.[58,60] However, in the present study the investigation using electron imaging paired with immunohistochemistry was limited by different fixation methodologies. Recent advances in the optical clearing method have provided the visualization of molecularly and immunologically labeled structures within large intact tissues in 3 dimensions and allow analysis of complex structures that are not contained within 2-dimensional planes.[61] Future studies using electron microscopy or optical clearing protocols in this animal model will provide novel structural insights into WM dysmaturaion and injury in patients with CHD.

Our study demonstrates that the piglet brain is a powerful model to study human WM development. The piglet also allows us to perform CPB during the neonatal period,[22,23] which causes specific pathological conditions in the developing brain with CHD.[13] However, because of the high costs involved, the present study using the piglet survival model with CPB had limitations regarding the number of animals used and the number of in vivo imaging experiments performed, as compared with rodent studies. The small sample size may affect statistical analyses such as the cutoff value or threshold in logistic regression modeling and cause-and-effect relationships between cellular events and FA changes. Our future studies using the model should provide more statistical power and improve our knowledge about the complex factors analyzed in this study such as different developmental time windows, various WM areas, and various brain insults associated with cardiac surgery. We used manual ROI measurements to determine DTI indices in the porcine WM. For further improvement of quantitative characterization in the model, development of a detailed WM atlas as established for the rodent brain[62] is also needed for the porcine brain. Although we accounted for multiple testing in the 31 WM regions imaged, cellular analyses in the present study was limited to 7 WM regions because of the labor-intensive and time-consuming nature of quantification of immunohistochemical assays using the piglet brain. Extending

our cellular assay in our future studies and defining the relationship between image biomarkers and cellular events to all WM regions of the piglet brain will undoubtedly enhance our understanding of complex WM development and injury after pediatric cardiac surgery.

It has been well documented that the presence of CHD in utero can induce WM dysmaturation resulting in immaturity at birth, which impacts the risk of subsequent injury.[7,63] Our piglet CPB model enabled us to reproduce unique surgery-related stresses to the neonatal human brain with CHD. However, the model does not take into account the potential impact of in utero development and pre-CPB injury to the WM, which likely alters the susceptibility to subsequent injury. Our recent study has identified several pathological signatures of the fetal human brain with CHD that can be reproduced and modeled with the developing piglet brain under chronic hypoxia.[20] A combined experimental paradigm using piglets exposed to both hypoxia and CPB will allow us to investigate the overall impact of CHD and subsequent cardiac surgery and will help further understanding of multietiological complex WM dysmaturation in the CHD population.

The present study showed that decreases of 20 and 40 mature oligodendrocytes (per 100 μm^3) are associated with a probability of FA reduction of 60% and 80%, respectively. Conversely an increase of 40 mature oligodendrocytes involves only 8% probability of CPB-induced FA reduction, suggesting that increasing mature oligodendrocyte number (eg, 40 mature oligodendrocytes per 100 μm^3) can be targeted to recover WM microstructural alterations after CPB. It has been well documented that the immature population in the oligodendrocyte lineage such as oligodendrocyte progenitors retains their mitotic and differentiation potential, as the brain is able to endogenously replenish damaged WM.[37,58,64–66] WM regions in the frontal cortex regions affected by severe CPB insults such as BCC, SFWM, or MFWM still contain significant numbers of immature oligodendrocytes at postoperative week 4. Our previous studies in both mouse and piglet models demonstrated that oligodendrocyte progenitor cells were resistant to CPB-induced insults.[22,67] Taken in conjunction, our study supports the concept that optimal treatment for successful WM development in CHD requires therapy aimed at promoting endogenous recovery through the action of oligodendrocyte progenitors including proliferation, differentiation, and myelination.

In summary, our study demonstrated that the piglet brain is a powerful model to study human WM development. FA changes after surgery are region specific and insult dependent and are associated with oligodendrocyte dysmaturation, astrogliosis, and microglial expansion. Reducing and recovering alterations of oligodendrocyte development in the frontal cortex can be targeted to improve lifelong neurodevelopmental consequences in the CHD population. Further studies in this model will provide exceptional data needed to interpret human imaging studies.

Acknowledgments

We are thankful to Dr Chung-Shieh Wu for assistance with MRI studies using the piglet model and to all our colleagues at the Center for Neuroscience Research for discussion and for their support. We thank colleagues of the Children's National Health System Research Animal Facility for their support with the porcine survival studies.

Sources of Funding

This work was partially supported by National Institutes of Health (NIH) grant R01HL060922, R01HL104173, R01HL128546, G12MD007597, and by a grant from the Children's Heart Foundation, the Baier Cardiac Research Fund, and the Foglia and Hills Families. Pham and Kumar were supported by the Gill Fellowship Program. This publication was also supported by Award Number 1U54HD090257-01 from the NIH, District of Columbia Intellectual and Developmental Disabilities Research Center Award (DC-IDDRC) program. Its contents are solely the responsibility of the authors and do not necessarily represent the official views of the DC-IDDRC or the NIH.

Disclosures

None.

References

1. Marino BS, Lipkin PH, Newburger JW, Peacock G, Gerdes M, Gaynor JW, Mussatto KA, Uzark K, Goldberg CS, Johnson WH Jr, Li J, Smith SE, Bellinger DC, Mahle WT. Neurodevelopmental outcomes in children with congenital heart disease: evaluation and management: a scientific statement from the American Heart Association. *Circulation*. 2012;126:1143–1172.
2. Gaynor JW, Stopp C, Wypij D, Andropoulos DB, Atallah J, Atz AM, Beca J, Donofrio MT, Duncan K, Ghanayem NS, Goldberg CS, Hovels-Gurich H, Ichida F, Jacobs JP, Justo R, Latal B, Li JS, Mahle WT, McQuillen PS, Menon SC, Pemberton VL, Pike NA, Pizarro C, Shekerdemian LS, Synnes A, Williams I, Bellinger DC, Newburger JW; International Cardiac Collaborative on Neurodevelopment Investigators. Neurodevelopmental outcomes after cardiac surgery in infancy. *Pediatrics*. 2015;135:816–825.
3. Bellinger DC, Wypij D, Rivkin MJ, DeMaso DR, Robertson RL Jr, Dunbar-Masterson C, Rappaport LA, Wernovsky G, Jonas RA, Newburger JW. Adolescents with d-transposition of the great arteries corrected with the arterial switch procedure: neuropsychological assessment and structural brain imaging. *Circulation*. 2011;124:1361–1369.
4. Morton PD, Ishibashi N, Jonas RA. Neurodevelopmental abnormalities and congenital heart disease: insights into altered brain maturation. *Circ Res*. 2017;120:960–977.
5. Galli KK, Zimmerman RA, Jarvik GP, Wernovsky G, Kuypers MK, Clancy RR, Montenegro LM, Mahle WT, Newman MF, Saunders AM, Nicolson SC, Spray TL, Gaynor JW. Periventricular leukomalacia is common after neonatal cardiac surgery. *J Thorac Cardiovasc Surg*. 2004;127:692–704.
6. Miller SP, McQuillen PS, Hamrick S, Xu D, Glidden DV, Charlton N, Karl T, Azakie A, Ferriero DM, Barkovich AJ, Vigneron DB. Abnormal brain development in newborns with congenital heart disease. *N Engl J Med*. 2007;357:1928–1938.

7. Andropoulos DB, Hunter JV, Nelson DP, Stayer SA, Stark AR, McKenzie ED, Heinle JS, Graves DE, Fraser CD Jr. Brain immaturity is associated with brain injury before and after neonatal cardiac surgery with high-flow bypass and cerebral oxygenation monitoring. *J Thorac Cardiovasc Surg*. 2010;139:543–556.
8. Lubsen J, Vohr B, Myers E, Hampson M, Lacadie C, Schneider KC, Katz KH, Constable RT, Ment LR. Microstructural and functional connectivity in the developing preterm brain. *Semin Perinatol*. 2011;35:34–43.
9. Mullen KM, Vohr BR, Katz KH, Schneider KC, Lacadie C, Hampson M, Makuch RW, Reiss AL, Constable RT, Ment LR. Preterm birth results in alterations in neural connectivity at age 16 years. *Neuroimage*. 2011;54:2563–2570.
10. Fields RD. White matter in learning, cognition and psychiatric disorders. *Trends Neurosci*. 2008;31:361–370.
11. Wernovsky G. Current insights regarding neurological and developmental abnormalities in children and young adults with complex congenital cardiac disease. *Cardiol Young*. 2006;16(suppl 1):92–104.
12. DeMaso DR, Labella M, Taylor GA, Forbes PW, Stopp C, Bellinger DC, Rivkin MJ, Wypij D, Newburger JW. Psychiatric disorders and function in adolescents with d-transposition of the great arteries. *J Pediatr*. 2014;165:760–766.
13. Morton PD, Ishibashi N, Jonas RA, Gallo V. Congenital cardiac anomalies and white matter injury. *Trends Neurosci*. 2015;38:353–363.
14. Mori S, Zhang J. Principles of diffusion tensor imaging and its applications to basic neuroscience research. *Neuron*. 2006;51:527–539.
15. Zhang J, Aggarwal M, Mori S. Structural insights into the rodent CNS via diffusion tensor imaging. *Trends Neurosci*. 2012;35:412–421.
16. Rivkin MJ, Watson CG, Scoppettuolo LA, Wypij D, Vajapeyam S, Bellinger DC, Demaso DR, Robertson RL Jr, Newburger JW. Adolescents with d-transposition of the great arteries repaired in early infancy demonstrate reduced white matter microstructure associated with clinical risk factors. *J Thorac Cardiovasc Surg*. 2013;146:543–549.e1.
17. Rollins CK, Watson CG, Asaro LA, Wypij D, Vajapeyam S, Bellinger DC, DeMaso DR, Robertson RL Jr, Newburger JW, Rivkin MJ. White matter microstructure and cognition in adolescents with congenital heart disease. *J Pediatr*. 2014;165:936–944.e1–2.
18. Clouchoux C, Limperopoulos C. Novel applications of quantitative MRI for the fetal brain. *Pediatr Radiol*. 2012;42(suppl 1):S24–S32.
19. Howells DW, Porritt MJ, Rewell SS, O'Collins V, Sena ES, van der Worp HB, Traystman RJ, Macleod MR. Different strokes for different folks: the rich diversity of animal models of focal cerebral ischemia. *J Cereb Blood Flow Metab*. 2010;30:1412–1431.
20. Morton PD, Korotcova L, Lewis BK, Bhuvanendran S, Ramachandra SD, Zurakowski D, Zhang J, Mori S, Frank JA, Jonas RA, Gallo V, Ishibashi N. Abnormal neurogenesis and cortical growth in congenital heart disease. *Sci Transl Med*. 2017;9:eaah7029.
21. Felix B, Leger ME, Albe-Fessard D, Marcilloux JC, Rampin O, Laplace JP. Stereotaxic atlas of the pig brain. *Brain Res Bull*. 1999;49:1–137.
22. Ishibashi N, Scafidi J, Murata A, Korotcova L, Zurakowski D, Gallo V, Jonas RA. White matter protection in congenital heart surgery. *Circulation*. 2012;125:859–871.
23. Korotcova L, Kumar S, Agematsu K, Morton PD, Jonas RA, Ishibashi N. Prolonged white matter inflammation after cardiopulmonary bypass and circulatory arrest in a juvenile porcine model. *Ann Thorac Surg*. 2015;100:1030–1037.
24. Levy JH, Tanaka KA. Inflammatory response to cardiopulmonary bypass. *Ann Thorac Surg*. 2003;75:S715–S720.
25. Schievink WI, Mokri B, Piepgras DG, Gittenberger-de Groot AC. Intracranial aneurysms and cervicocephalic arterial dissections associated with congenital heart disease. *Neurosurgery*. 1996;39:685–689; discussion 689–690.
26. Jonas RA. Deep hypothermic circulatory arrest: current status and indications. *Semin Thorac Cardiovasc Surg Pediatr Card Surg Annu*. 2002;5:76–88.
27. Hickey PR. *Endothelial and White Cell Activation in Bypass and Reperfusion Injury: Brain Injury*. 1st ed. Newton: Butterworth-Heinemann; 1996.
28. Shin'oka T, Shum-Tim D, Jonas RA, Lidov HG, Laussen PC, Miura T, du Plessis A. Higher hematocrit improves cerebral outcome after deep hypothermic circulatory arrest. *J Thorac Cardiovasc Surg*. 1996;112:1610–1620; discussion 1620–1621.
29. Wypij D, Jonas RA, Bellinger DC, Del Nido PJ, Mayer JE Jr, Bacha EA, Forbess JM, Pigula F, Laussen PC, Newburger JW. The effect of hematocrit during hypothermic cardiopulmonary bypass in infant heart surgery: results from the combined Boston hematocrit trials. *J Thorac Cardiovasc Surg*. 2008;135:355–360.
30. Sakamoto T, Zurakowski D, Duebener LF, Lidov HG, Holmes GL, Hurley RJ, Laussen PC, Jonas RA. Interaction of temperature with hematocrit level and pH determines safe duration of hypothermic circulatory arrest. *J Thorac Cardiovasc Surg*. 2004;128:220–232.
31. Aoki M, Nomura F, Stromski ME, Tsuji MK, Fackler JC, Hickey PR, Holtzman DH, Jonas RA. Effects of pH on brain energetics after hypothermic circulatory arrest. *Ann Thorac Surg*. 1993;55:1093–1103.
32. du Plessis AJ, Jonas RA, Wypij D, Hickey PR, Riviello J, Wessel DL, Roth SJ, Burrows FA, Walter G, Farrell DM, Walsh AZ, Plumb CA, del Nido P, Burke RP, Castaneda AR, Mayer JE Jr, Newburger JW. Perioperative effects of alpha-stat versus pH-stat strategies for deep hypothermic cardiopulmonary bypass in infants. *J Thorac Cardiovasc Surg*. 1997;114:991–1000; discussion 1000–1001.
33. Ishibashi N, Iwata Y, Okamura T, Zurakowski D, Lidov HG, Jonas RA. Differential neuronal vulnerability varies according to specific cardiopulmonary bypass insult in a porcine survival model. *J Thorac Cardiovasc Surg*. 2010;140:1408–1415.e3.
34. Pierpaoli C, Walker L, Irfanoglu MO, Barnett A, Basser P, Chang L-C, Koay C, Pajevic S, Rohde G, Sarlls J, Wu M. TORTOISE: an integrated software package for processing of diffusion MRI data. Paper presented at: ISMRM 18th annual meeting. Stockholm, Sweden; 2010.
35. Oishi K, Zilles K, Amunts K, Faria A, Jiang H, Li X, Akhter K, Hua K, Woods R, Toga AW, Pike GB, Rosa-Neto P, Evans A, Zhang J, Huang H, Miller MI, van Zijl PC, Mazziotta J, Mori S. Human brain white matter atlas: identification and assignment of common anatomical structures in superficial white matter. *Neuroimage*. 2008;43:447–457.
36. Back SA. Perinatal white matter injury: the changing spectrum of pathology and emerging insights into pathogenetic mechanisms. *Ment Retard Dev Disabil Res Rev*. 2006;12:129–140.
37. Aguirre A, Dupree JL, Mangin JM, Gallo V. A functional role for EGFR signaling in myelination and remyelination. *Nat Neurosci*. 2007;10:990–1002.
38. Gundersen HJ, Bagger P, Bendtsen TF, Evans SM, Korbo L, Marcussen N, Moller A, Nielsen K, Nyengaard JR, Pakkenberg B, Sorensen FB, Vesterby A, West MJ. The new stereological tools: disector, fractionator, nucleator and point sampled intercepts and their use in pathological research and diagnosis. *APMIS*. 1988;96:857–881.
39. Cabral HJ. Multiple comparisons procedures. *Circulation*. 2008;117:698–701.
40. Back SA, Luo NL, Borenstein NS, Levine JM, Volpe JJ, Kinney HC. Late oligodendrocyte progenitors coincide with the developmental window of vulnerability for human perinatal white matter injury. *J Neurosci*. 2001;21:1302–1312.
41. Kinney HC, Brody BA, Kloman AS, Gilles FH. Sequence of central nervous system myelination in human infancy. II. Patterns of myelination in autopsied infants. *J Neuropathol Exp Neurol*. 1988;47:217–234.
42. Seber GAF, Wild CJ. *Nonlinear Regression*. New York: John Wiley & Sons; 2003.
43. Geng X, Gouttard S, Sharma A, Gu H, Styner M, Lin W, Gerig G, Gilmore JH. Quantitative tract-based white matter development from birth to age 2 years. *Neuroimage*. 2012;61:542–557.
44. Oishi K, Faria AV, Yoshida S, Chang L, Mori S. Quantitative evaluation of brain development using anatomical MRI and diffusion tensor imaging. *Int J Dev Neurosci*. 2013;31:512–524.
45. Oishi K, Mori S, Donohue PK, Ernst T, Anderson L, Buchthal S, Faria A, Jiang H, Li X, Miller MI, van Zijl PC, Chang L. Multi-contrast human neonatal brain atlas: application to normal neonate development analysis. *Neuroimage*. 2011;56:8–20.
46. Thiebaut de Schotten M, Dell'Acqua F, Forkel SJ, Simmons A, Vergani F, Murphy DG, Catani M. A lateralized brain network for visuospatial attention. *Nat Neurosci*. 2011;14:1245–1246.
47. Back SA, Gan X, Li Y, Rosenberg PA, Volpe JJ. Maturation-dependent vulnerability of oligodendrocytes to oxidative stress-induced death caused by glutathione depletion. *J Neurosci*. 1998;18:6241–6253.
48. Riddle A, Luo NL, Manese M, Beardsley DJ, Green L, Rorvik DA, Kelly KA, Barlow CH, Kelly JJ, Hohimer AR, Back SA. Spatial heterogeneity in oligodendrocyte lineage maturation and not cerebral blood flow predicts fetal ovine periventricular white matter injury. *J Neurosci*. 2006;26:3045–3055.
49. Agematsu K, Korotcova L, Morton PD, Gallo V, Jonas RA, Ishibashi N. Hypoxia diminishes the protective function of white-matter astrocytes in the developing brain. *J Thorac Cardiovasc Surg*. 2016;151:265–272.e1–3.
50. Xie M, Tobin JE, Budde MD, Chen CI, Trinkaus K, Cross AH, McDaniel DP, Song SK, Armstrong RC. Rostrocaudal analysis of corpus callosum demyelination and axon damage across disease stages refines diffusion tensor imaging correlations with pathological features. *J Neuropathol Exp Neurol*. 2010;69:704–716.
51. Zhang J, Jones MV, McMahon MT, Mori S, Calabresi PA. In vivo and ex vivo diffusion tensor imaging of cuprizone-induced demyelination in the mouse corpus callosum. *Magn Reson Med*. 2012;67:750–759.
52. Bargmann CI, Newsome WT. The Brain Research Through Advancing Innovative Neurotechnologies (BRAIN) initiative and neurology. *JAMA Neurol*. 2014;71:675–676.

53. Wilson CR, Gaffan D, Browning PG, Baxter MG. Functional localization within the prefrontal cortex: missing the forest for the trees? *Trends Neurosci*. 2010;33:533–540.

54. Blakemore SJ, Robbins TW. Decision-making in the adolescent brain. *Nat Neurosci*. 2012;15:1184–1191.

55. Baluch F, Itti L. Mechanisms of top-down attention. *Trends Neurosci*. 2011;34:210–224.

56. Luu TM, Ment L, Allan W, Schneider K, Vohr BR. Executive and memory function in adolescents born very preterm. *Pediatrics*. 2011;127:e639–e646.

57. McCrindle BW, Williams RV, Mitchell PD, Hsu DT, Paridon SM, Atz AM, Li JS, Newburger JW. Relationship of patient and medical characteristics to health status in children and adolescents after the Fontan procedure. *Circulation*. 2006;113:1123–1129.

58. Scafidi J, Hammond TR, Scafidi S, Ritter J, Jablonska B, Roncal M, Szigeti-Buck K, Coman D, Huang Y, McCarter RJ Jr, Hyder F, Horvath TL, Gallo V. Intranasal epidermal growth factor treatment rescues neonatal brain injury. *Nature*. 2014;506:230–234.

59. Forster R, Bode G, Ellegaard L, van der Laan JW. The RETHINK project on minipigs in the toxicity testing of new medicines and chemicals: conclusions and recommendations. *J Pharmacol Toxicol Methods*. 2010;62:236–242.

60. Favrais G, van de Looij Y, Fleiss B, Ramanantsoa N, Bonnin P, Stoltenburg-Didinger G, Lacaud A, Saliba E, Dammann O, Gallego J, Sizonenko S, Hagberg H, Lelievre V, Gressens P. Systemic inflammation disrupts the developmental program of white matter. *Ann Neurol*. 2011;70:550–565.

61. Chung K, Wallace J, Kim SY, Kalyanasundaram S, Andalman AS, Davidson TJ, Mirzabekov JJ, Zalocusky KA, Mattis J, Denisin AK, Pak S, Bernstein H, Ramakrishnan C, Grosenick L, Gradinaru V, Deisseroth K. Structural and molecular interrogation of intact biological systems. *Nature*. 2013;497:332–337.

62. Chuang N, Mori S, Yamamoto A, Jiang H, Ye X, Xu X, Richards LJ, Nathans J, Miller MI, Toga AW, Sidman RL, Zhang J. An MRI-based atlas and database of the developing mouse brain. *Neuroimage*. 2011;54:80–89.

63. Beca J, Gunn JK, Coleman L, Hope A, Reed PW, Hunt RW, Finucane K, Brizard C, Dance B, Shekerdemian LS. New white matter brain injury after infant heart surgery is associated with diagnostic group and the use of circulatory arrest. *Circulation*. 2013;127:971–979.

64. Gage FH, Temple S. Neural stem cells: generating and regenerating the brain. *Neuron*. 2013;80:588–601.

65. Gallo V, Armstrong RC. Myelin repair strategies: a cellular view. *Curr Opin Neurol*. 2008;21:278–283.

66. Etxeberria A, Mangin JM, Aguirre A, Gallo V. Adult-born SVZ progenitors receive transient synapses during remyelination in corpus callosum. *Nat Neurosci*. 2010;13:287–289.

67. Agematsu K, Korotcova L, Scafidi J, Gallo V, Jonas RA, Ishibashi N. Effects of preoperative hypoxia on white matter injury associated with cardiopulmonary bypass in a rodent hypoxic and brain slice model. *Pediatr Res*. 2014;75:618–625.

Microstructural Alterations and Oligodendrocyte Dysmaturation in White Matter After Cardiopulmonary Bypass in a Juvenile Porcine Model

Gary R. Stinnett, Stephen Lin, Alexandru V. Korotcov, Ludmila Korotcova, Paul D. Morton, Shruti D. Ramachandra, Angeline Pham, Sonali Kumar, Kota Agematsu, David Zurakowski, Paul C. Wang, Richard A. Jonas and Nobuyuki Ishibashi

J Am Heart Assoc. 2017;6:e005997; originally published August 15, 2017;
doi: 10.1161/JAHA.117.005997
The *Journal of the American Heart Association* is published by the American Heart Association, 7272 Greenville Avenue, Dallas, TX 75231
Online ISSN: 2047-9980